

THESIS

A MODELING TOOL FOR HOUSEHOLD BIOGAS BURNER FLAME PORT DESIGN

Submitted by

Thomas J. Decker

Department of Mechanical Engineering

In partial fulfillment of the requirements

For the Degree of Master of Science

Colorado State University

Fort Collins, Colorado

Summer 2017

Master's Committee:

Advisor: Thomas Bradley

Jason Prapas

Sybil Sharvelle

Copyright by Thomas J Decker 2017

All Rights Reserved

ABSTRACT

A MODELING TOOL FOR HOUSEHOLD BIOGAS BURNER FLAME PORT DESIGN

Anaerobic digestion is a well-known and potentially beneficial process for rural communities in emerging markets, providing the opportunity to generate usable gaseous fuel from agricultural waste. With recent developments in low-cost digestion technology, communities across the world are gaining affordable access to the benefits of anaerobic digestion derived biogas. For example, biogas can displace conventional cooking fuels such as biomass (wood, charcoal, dung) and Liquefied Petroleum Gas (LPG), effectively reducing harmful emissions and fuel cost respectively.

To support the ongoing scaling effort of biogas in rural communities, this study has developed and tested a design tool aimed at optimizing flame port geometry for household biogas-fired burners. The tool consists of a multi-component simulation that incorporates three-dimensional CAD designs with simulated chemical kinetics and computational fluid dynamics. An array of circular and rectangular port designs was developed for a widely available biogas stove (called the *Lotus*) as part of this study. These port designs were created through guidance from previous studies found in the literature. The three highest performing designs identified by the tool were manufactured and tested experimentally to validate tool output and to compare against the original port geometry. The experimental results aligned with the tool's prediction for the three chosen designs. Each design demonstrated improved thermal efficiency relative to the original, with one configuration of circular ports exhibiting superior performance. The results of the study indicated that designing for a targeted range of port hydraulic diameter, velocity and mixture

density in the tool is a relevant way to improve the thermal efficiency of a biogas burner. Conversely, the emissions predictions made by the tool were found to be unreliable and incongruent with laboratory experiments.

ACKNOWLEDGMENTS

Over the past two years, I have learned and grown more than I could have imagined. From mechanical engineering principles to entrepreneurship and design, Colorado State has been a one of a kind experience. I would like to first thank Jason Prapas for his mentorship, support, technical direction and exposure to professional development opportunities. I would not have had the graduate experience that I did without your guidance and friendship. Thanks go out to Tom Bradley and Marc Baumgardner for providing research expertise and keeping me on the straight and narrow. Special thanks to Marc for his contributions of research and combustion knowledge. I would like to thank Sybil Sharvelle for joining my committee and to John Mizia, James Tillotson, Christian L'Orange and Anthony Marchese among others who contributed to this work. Thanks to my friends and family who supported me through this time and kept me sane when I wondered how I fit into this world of ours. Thank you to the National Science Foundation Graduate Research Fellowship Program for funding my time at Colorado State and to Factor[e] Ventures and Sistema Biobolsa for supporting this study as well as my professional growth and education.

Last, but certainly not least, I owe a great deal of gratitude to my girlfriend, Alycia, who has stood by my side for the past eight years and admirably continues to indulge in my adventures.

TABLE OF CONTENTS

ABSTRACT.....	ii
ACKNOWLEDGMENTS	iv
LIST OF TABLES	viii
LIST OF FIGURES	ix
CHAPTER 1. INTRODUCTION AND BACKGROUND	1
1.1 The Problem.....	1
1.2 Project Background.....	2
1.3 Biogas Utilization	2
1.4 Biogas Combustion.....	2
1.4.1 Flame Type	3
1.5 Burner Design	5
1.5.1 Flame Port Geometry	7
1.6 Biogas Burner Development.....	9
1.7 Research Summary and Hypotheses.....	11
CHAPTER 2. DESIGN AND MODELING METHODS	13
2.1 Flame Port Design.....	13
2.2 Biogas Composition.....	15
2.2.1 Laboratory Evaluation	15
2.2.2 Field Evaluation	17
2.3 Modeling.....	18
2.3.1 3-D Assemblies.....	20
2.3.2 Chemical Kinetics Calculations.....	21
2.3.3 Computational Fluid Dynamics Simulation.....	23
2.3.3.1 Burner Assembly Mixing Simulation	23
2.3.3.2 Flame Port Combustion Simulation	24
2.3.4 Port Design Rank	25
CHAPTER 3. EXPERIMENT SETUP AND METHODS.....	27
3.1 Experiment Overview	27
3.2 Experiment Setup.....	27
3.2.1 Biogas Supply	27
3.2.2 Biogas Flow Control.....	29

3.2.3	Sampling Equipment.....	30
3.2.3.1	Laminar Flow Hood	31
3.2.3.2	Supervisory Control and Data Acquisition (SCADA)	32
3.2.3.3	Gaseous Emissions.....	33
3.2.3.4	Particulate Matter Emissions.....	34
3.2.4	Design Manufacturing	36
3.2.5	Testing Protocol	38
3.2.5.1	Flame Color Analysis.....	41
3.2.6	Off the Shelf Burner Testing.....	42
CHAPTER 4.	RESULTS AND DISCUSSION.....	43
4.1	Modeling Tool	43
4.1.1	Burner Assembly Mixing Simulation	43
4.1.1.1	Visual Representations	45
4.1.2	Flame Port Combustion Simulation.....	46
4.1.2.1	Emissions	47
4.1.2.2	Temperatures	47
4.1.2.3	Visual Representations	48
4.1.3	Port Geometry.....	50
4.1.4	Port Spacing.....	54
4.1.5	Port Design Rank	55
4.2	Experiment.....	56
4.2.1	Off the Shelf Burner Testing.....	57
4.2.1.1	Influence of Flame Type	57
4.2.1.2	Influence of Firepower	59
4.2.1.3	Particulate Matter Emissions.....	60
4.2.2	Time Controlled Protocol	61
4.2.2.1	Low Firepower Condition	61
4.2.2.2	Firepower Sweep.....	70
4.2.3	Temperature Controlled Protocol	73
CHAPTER 5.	CONCLUSION	75
5.1	Summary of Findings.....	75
5.2	Original Hypotheses.....	76
5.3	Future Work	77
5.3.1	Modeling Tool Development.....	77

5.3.2 Experiments	78
5.3.3 Flame Port Design.....	79
BIBLIOGRAPHY.....	81
APPENDIX A. SUPPLEMENTARY MATERIAL FOR CHAPTERS 1, 2 AND 3.....	84
APPENDIX B. SUPPLEMENTARY MATERIAL FOR CHAPTER 4	92

LIST OF TABLES

Table 1 – Propane and biogas energy density values	6
Table 2 – Flame port design dimensions and descriptions	14
Table 3 – Laboratory biodigester composition results.....	16
Table 4 – Results of the field evaluation of biogas composition in Gujarat, India.....	17
Table 5 – Pressure outlet initial mass fraction guesses.....	24
Table 6 – Boundary tab species mass fraction of species in air.....	24
Table 7 – Equipment and instruments to complete the experiment.....	31
Table 8 – Equivalence ratio and average port velocity results used to inform the combustion simulation.....	44
Table 9 – Results from the flame port combustion simulation.....	46
Table 10 – Relationship strength indicators for the influence of factors upon the model predictors	53
Table 11 – Results of the equal weighted ranking procedure to determine the top three designs	56
Table 12 – Thermal efficiency summary	62
Table 13 – Summary of predictor variables describing each of the experimentally tested designs	64
Table 14 – Compared percent error of model and experimental emissions results	66
Table 15 – Lookup table produced by Chemkin for a 60 mole percent biogas	84
Table 16 – Summary of particulate matter results	92
Table 17 – Delher LPG stove modifications for biogas	93
Table 18 – Delher scenario ranking comparison	95

LIST OF FIGURES

Figure 1 – Primary energy source for cooking in house-holds in India and Botswana [6].	1
Figure 2 – Common burner configuration [14].	5
Figure 3 – Combustion diagram for a typical aerated burner [14]	7
Figure 4 – Flow diagram of variable inter-dependence and contribution to Reynolds number	8
Figure 5 – Approach concept combining design, modeling and experiments	11
Figure 6 – Original Lotus biogas burner flame port design	13
Figure 7 – Mobile biodigester experiment	15
Figure 8 – Gas sampling set up, pump and sealed sample bag	16
Figure 9 – Biogas 5000 portable infrared and electrochemical analyzer	17
Figure 10 – Process flow diagram of the modeling tool	19
Figure 11 – Lotus burner assembly, complete and halved	20
Figure 12 – Flame ports and external volume model	21
Figure 13 – Adiabatic flame temperature and laminar flame speed were modeled in Chemkin as a function of equivalence ratio. (Produced using the GRI 3.0 Mechanism)	23
Figure 14 – Synthetic 60 mole % methane, 40 mole % carbon dioxide biogas blend in a pressurized cylinder	28
Figure 15 – Combined with a cylinder scale, the regulator provides flow control adjustment while the Magnehelic gauges provide supply pressure monitoring	30
Figure 16 – Diagram of the flow hood, particulate matter control and collection system and the gaseous emissions NDIR analyzer	32
Figure 17 – Far left: Manages pump speed and water temperature, Middle: Manages NDIR results, Far right: Manages temperature and pressure compensation	33
Figure 18 – PALL filters were created and equilibrated to measure particulate matter emissions from biogas burners	35
Figure 19 – A design specification sheet for Cap 1a of the developed flame port geometry designs	37
Figure 20 – Left: Part formation from laser fused metal powder, Right: Part curing in a kiln to achieve product durability [40]	37
Figure 21 – Left: Gas fired water boil test, Right: Wood fired water boil test	39
Figure 22 – Left: Measuring 5L of water, Right: Placement of an Omega K-Type thermocouple through the pot lid for the duration of each test	41
Figure 23 – A visualization of the entrainment effect of air and extent of homogeneity in the mixture for design 1a	45
Figure 24 – Velocity contours and vectors illustrating the entrainment of ambient air into the burner throat for a partially premixed flame for design 1a	46
Figure 25 – Top: CO and CH ₄ emissions comparison for all nine designs against the original, Bottom: Changes in combustion efficiency due to port geometry compared to the original design	47
Figure 26 – The influence of port geometry design changes on zone and maximum temperatures	48
Figure 27 – Temperature contour due to combustion within design 1a	49

Figure 28 – Velocity contours for design 1a showing a parabolic condition within circular ports	49
Figure 29 – Port shape ratio factor as a function of hydraulic diameter (D_h)	50
Figure 30 – Display proving the direct and linear relationship between bulk mass flow rate and mixture density with equivalence ratio	51
Figure 31 – Matlab® rstool prediction profiler to establish a design response surface for desired predictor values	53
Figure 32 – Results of a multiple linear regression: $\ln(\text{Reynolds} \sim D_h + \text{velocity} + \rho_{\text{mixture}})$	54
Figure 33 – A display of wide variations and little to no correlation between port spacing and performance predictors	55
Figure 34 – Left: Partially premixed flame, Right: Diffusion flame	57
Figure 35 – Upper firepower flame type comparison water boil tests using the IWA tier structure	58
Figure 36 – Lower firepower flame type comparison WBT for the Lotus burner	59
Figure 37 – An exploration of the influence of firepower on emissions and heat transfer.....	60
Figure 38 – Thermal efficiency results from the time controlled, low firepower condition	62
Figure 39 – Identical flame photos of each design providing for qualitative and quantitative analysis.....	63
Figure 40 – Experimental emissions results for each flame port design	64
Figure 41 – A graphical comparison of model and experimental emissions results	67
Figure 42 – A graphical comparison of model and experimental thermal results	68
Figure 43 – Lower firepower time controlled design comparison using the IWA tier structure..	70
Figure 44 – Sweep thermal efficiency data overlain with best fit trendlines.....	71
Figure 45 – Sweep emissions data overlain with linear trendlines.....	72
Figure 46 – Firepower sweep time controlled design comparison using the IWA tier structure .	73
Figure 47 – A percent error comparison of the temperature and time controlled protocol	74
Figure 48 – Delher LPG modification IWA tier comparison	94

CHAPTER 1. INTRODUCTION AND BACKGROUND

1.1 The Problem

Worldwide, nearly 2.7 billion people rely on the traditional use of biomass for daily cooking, leading to avoidable illness and pre-mature death [1]. The majority of this population (90%) is involved in smallholder agriculture and has access to agricultural waste that can be transformed into biogas, a sustainable methane based fuel [2]. Biogas has the potential to offset energy costs incurred by households for cooking, which is currently dominated by biomass, Liquefied Petroleum Gas (LPG) and kerosene (Figure 1) [3]. Health and climate costs of biomass emissions can also be abated through the adoption and use of biogas [4], [5].

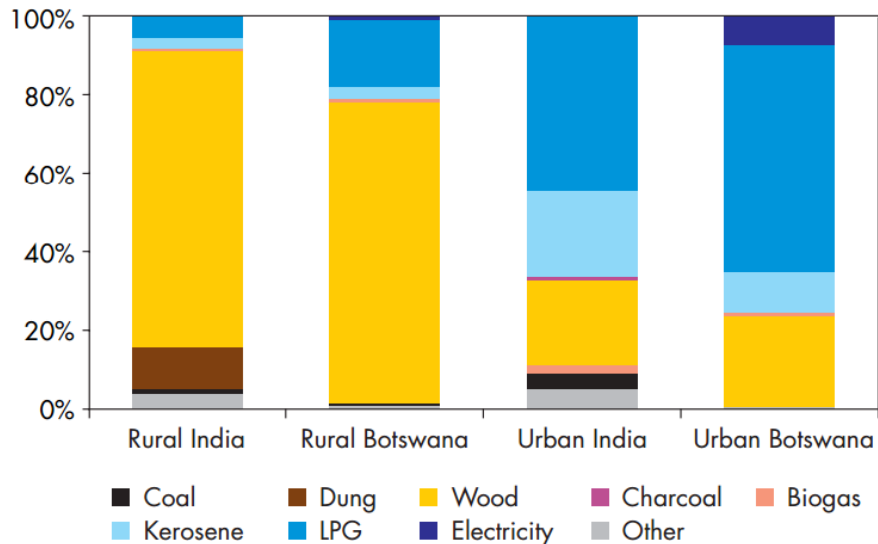


Figure 1 – Primary energy source for cooking in house-holds in India and Botswana [6].

Adoption rates for decentralized biodigesters, however, are low in emerging markets (< 50%) [7]. Studies have indicated that this low technology adoption is mainly due to low ambient temperature (< 10° C, resulting in reduced gas yield), feedstock issues, installation cost and complexity, low quality of gas production (methane content lower than 40 mole %), a lack of finance options and insufficient choices and low efficiencies of downstream use appliances [7].

1.2 Project Background

While working with biogas entrepreneurs, improving biogas cookstove performance was determined to be a point of significant impact, given that cooking is the most common use case of biogas among rural customers. Housed at the Powerhouse Energy Campus of Colorado State University, this study had access to cookstove design and evaluation facilities and was well suited to engage in such work. The results of the study are anticipated to impact biogas cookstove users throughout the world.

1.3 Biogas Utilization

For decentralized biodigesters, biogas is often most efficiently utilized as thermal energy for cooking ($\eta_{TH} \approx 45 - 55\%$), followed by electrical energy through combustion engines ($\eta_{TH} \approx 24\%$) and lighting in lamps ($\eta_{TH} \approx 3\%$) [8]. For industrial applications, biogas can be used as a fuel in combined heat and power technology ($\eta_{TH} \approx 88\%$) [8].

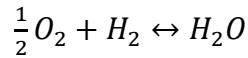
Biogas has specific characteristics that impact the performance of off-the-shelf appliances designed for LPG or other gaseous fuels. Biogas has lower energy density than conventional fuels (~ 21 MJ/kg), is supplied at low and varying pressures (often less than 0.5 psi) and includes water vapor and hydrogen sulfide that can lead to significant appliance corrosion over time. With the appropriate design measures in place, biogas has demonstrated the potential to be used for water and space heating, cooking, refrigeration, electricity generation or mechanical work [9].

1.4 Biogas Combustion

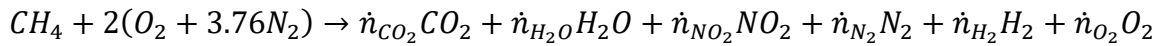
Biogas is typically comprised of an average of 50-75% methane and 25-50% carbon dioxide with trace amounts of water vapor, hydrogen sulfide, nitrogen, oxygen and ammonia [8]. Methane in biogas reacts with oxygen in air and triggers a series of steps in which the saturated compounds (those with a net zero valence number) of carbon dioxide and water are the main and

preferred products. Other products in significant quantities include H_2 , O_2 , N_2 , NO_2 , OH and CO . These are only some of the products, since chemical equilibrium requires a statistical distribution of the infinite number of molecular configurations of carbon, hydrogen and oxygen [10]. The canonical combustion of methane in air can be described by the reaction summary below. The mole fractions for each product are a function of temperature and pressure and a result of intermediate reactions such as the example for water formation listed below.

H_2O Formation:



Reaction Summary:



Given an average methane content of 60 mole percent in biogas and an oxygen content in air of 21 mole percent, the stoichiometric molar ratio of air and biogas is 5.70 to 1.

$$\frac{1 \text{ mole of methane}}{x \text{ moles of biogas}} = \frac{0.6 \text{ moles of methane}}{1 \text{ mole of biogas}} \rightarrow 1.67 \text{ moles of biogas}$$

$$\frac{2 \text{ moles of oxygen}}{x \text{ moles of air}} = \frac{0.21 \text{ moles of oxygen}}{1 \text{ moles of air}} \rightarrow 9.52 \text{ moles of air}$$

$$\frac{\text{moles of air}}{\text{moles of biogas}} = \frac{9.52}{1.67} = 5.70$$

1.4.1 Flame Type

Biogas can be combusted in household burners through non-premixed (diffusion) or partially pre-mixed flames. In either case, a concern of biogas combustion is flame liftoff. Flame liftoff occurs when the velocity of the gas and air mixture exiting a port is higher than the laminar flame speed, and flashback happens when the opposite occurs. Liftoff tendency is heightened in biogas burners due to the large percentage of inert gas (carbon dioxide) in the fuel, which reduces

the flame speed. When flame liftoff occurs, carbon monoxide and unburned hydrocarbon emissions increase due to incomplete combustion, leading to decreases in efficiency.

Non-premixed fuel diffuses with oxygen at the reaction zone and can be subject to large inrushes of oxygen, or over-ventilation, leading to flame stretch and extension of the stoichiometric mixture front [11]. Such stretch lowers the reaction rate as well as the laminar flame speed, leading to a greater chance of flame lift. Diffusion flames exhibit a yellow color due to the dominance of soot formation and consequently destruction in the reaction zone over also present excited C_2 and CH radicals [12]. If soot escapes the reaction zone, the particles appear as black smoke.

Partially pre-mixed flames are a result of fuel mixed with a portion of the stoichiometric oxygen requirement from an entrainment effect prior to the reaction zone. The entrainment effect is due to an induced drop in pressure after the injector (Figure 2). Premixed flames have a narrow reaction zone which leads to a higher reaction rate, or rate of reactant consumption as compared to diffusion [11]. A higher reaction rate leads to higher flame speeds and reduced occurrence of flame lift. Premixed flames exhibit a blue-green or violet color due to the chemiluminescence of excited species (C_2 and CH radicals).

Overall, domestic gas burners are generally designed to incorporate laminar partially premixed flames to reduce soot formation and encourage higher reaction rates [12]. Well-recognized combustion expert Irvin Glassman states that according to experiment and observation, "...the primary mixing processes of fuel and oxidizer appear to dominate the burning processes in diffusion flames" and "...the consumption and heat release rates of premixed flames are much larger than those of pure mixing controlled diffusion flames" [11]. Additionally, research conducted by Daniel Zube at Colorado State University showed higher thermal efficiencies when using a premixed flame in a Bunsen burner compared to a diffusion flame in the same burner [13].

1.5 Burner Design

A common household burner in which biogas can be combusted is composed of the following components: a control valve, injector, mixing tube and burner head.

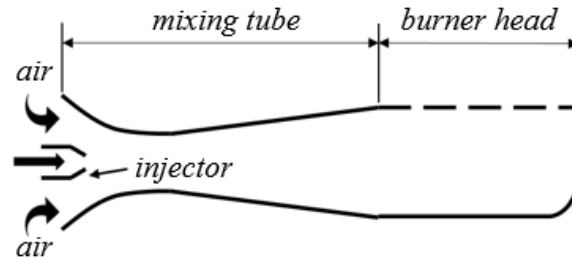


Figure 2 – Common burner configuration [14]

Burner design is influenced by the type of fuel used. Different fuels have varying rates of combustion and oxidizer requirements, leading to changes in the design of the injector and burner head. The lower heating value of the fuel directly determines the required mass flow rate to be provided to the burner head in order to maintain a desired firepower.

$$\text{Firepower [W]} = \frac{\text{fuel consumed [g]}}{\text{duration of test [s]}} * \text{Lower Heating Value} \left[\frac{\text{J}}{\text{g}} \right]$$

For example, the mass flow rate of propane will be lower than biogas to achieve the same firepower (Table 1). Thus, injector and flame port diameters are often smaller for LPG or propane burners as compared to biogas burners. In addition, the Wobbe number is a metric that describes heat output and can be used to compare varying gaseous fuels for a given system design.

$$\text{Wobbe \#} = \frac{\text{Higher Heating Value}}{\sqrt{\text{Specific Gravity}}}$$

In Table 1, the Wobbe number was used to show that at the same pressure, mass flow rate and burner dimensions, propane would be expected to output roughly 1.6 times the energy as biogas.

Table 1 – Propane and biogas energy density values

Type of Gas	Lower Heating Value (MJ/kg)	Wobbe Number in Colorado (MJ/kg)
Propane	46.35	37.72
60 mole % Methane Biogas	22.65	23.91

Area ratios between stove components can help a designer hone in on the optimal geometry for a burner. Such ratios include mixing tube cross sectional area to total port area, injector orifice cross sectional area to mixing tube cross sectional area and injector orifice cross sectional area to total port area. Additionally, mixing tubes should have a length to diameter ratio of 10-12 [14]. The actual area ratios from burner dimensions can be compared to the optimal ratios calculated from the following equations where C_{dp} is the port discharge coefficient (0.6-0.7), C_L is the loss coefficient representing losses in the mixing tube and burner head (0.25-0.35), SG is the specific gravity of biogas (0.897 in Colorado) and R is the entrainment ratio which is the primary air entrained divided by the driving flow [14].

$$\frac{A_{mixing\ tube}}{A_{ports}} = C_{dp} \sqrt{1 + C_L}$$

$$\frac{A_{injector}}{A_{mixing\ tube}} = \frac{SG}{(SG + R) * (1 + R) * (1 + C_L)}$$

$$\frac{A_{injector}}{A_{port}} = \frac{SG * C_{dp}}{(SG + R) * (1 + R) * (1 + C_L)}$$

Often, burner design revolves around a desired entrainment ratio, which needs to be determined so that there is not a tendency for flashback (low aeration) or liftoff (high aeration) (Figure 3) [14]. If required, a flame can be stable at high aerations and high port loading with the inclusion of retention flames.

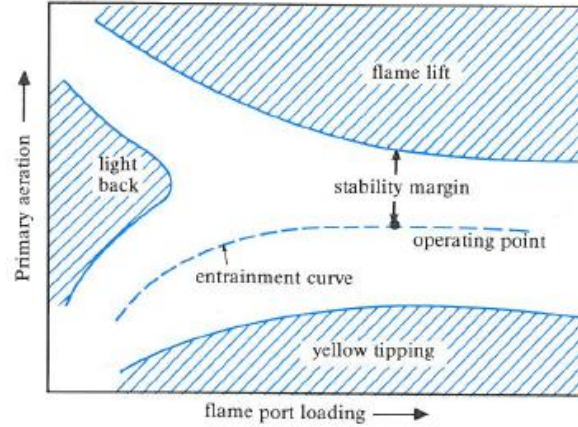


Figure 3 – Combustion diagram for a typical aerated burner [14]

1.5.1 Flame Port Geometry

The flame port is one of several burner components that conveys and defines the flow of a fuel mixture before ignition. By changing the geometry, or hydraulic diameter (including the actual diameter, length and width) of the flame port, the gas flow rate, mixture density ($\rho_{mixture}$) and velocity also change. Geometry change influences gas mixture density through the effect of the back pressure of each design on the amount of entrained air into a constant stream of fuel. As bulk mass flow rate and consequently mixture density changes, velocity changes as shown in the continuity equation:

$$v_{inlet} \left[\frac{m}{s} \right] = \frac{\dot{m}_{bulk\ flow} \left[\frac{kg}{s} \right]}{A_{XS,ports} [m^2] * \rho_{mixture} \left[\frac{kg}{m^3} \right]}$$

Geometry changes hydraulic diameter through varying cross sectional area and wetted perimeter.

$$D_h = 4 * \frac{A_{cross\ sectional}}{P_{wetted}}$$

To unify the multiple contributing variables described above to explain flow pattern, Reynolds number was developed. Reynolds number utilizes velocity, gas mixture density and hydraulic diameter to help predict flow patterns and differentiate between laminar and turbulent flow.

$$Re = \frac{D_h [m] * v \left[\frac{m}{s} \right] * \rho_{mixture} \left[\frac{kg}{m^3} \right]}{dynamic\ viscosity [Pa * s]}$$

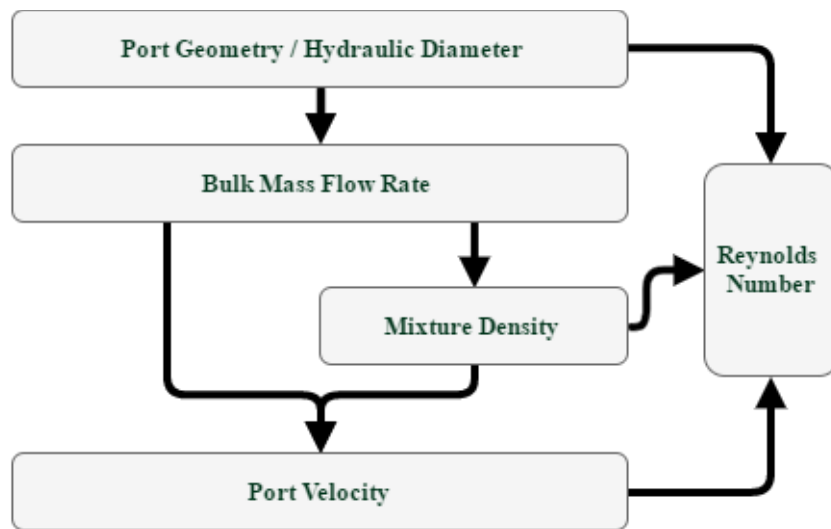


Figure 4 – Flow diagram of variable inter-dependence and contribution to Reynolds number

Beyond these fundamental variables, there are several influential geometric factors to consider. These include flow path surface area as determined by port depth ratios, sharp edges and corners that can cause localized turbulence and port to port spacing that defines inter-port temperatures. A mid to late 20th century summary of LPG and natural gas research by H.R.N. Jones recommends less than six mm inter-port spacing, a port depth to diameter ratio of greater than two, and a greater than four to one ratio of length to width for rectangular ports [14]. Such recommendations stem from research conducted by Griffiths and Weber and Harris and South to limit flame lift and test the influence of geometry on flame structure [15], [16]. Other recent LPG and natural gas studies have investigated the influence of circular port diameter, port inclination

to test swirl influence, port to port spacing, ribbon patterns and the performance of the conventional radial flow slotted (CB), new swirl flow (NB), radiant (RB) and swirling central (SB) burners [17]–[19]. Flame port designs have also been patented by General Electric using rectangular slots and flared flame retention ports [20].

Biogas flame port research is less comprehensive in comparison. In a biogas burner design manual, Fulford writes about circular flame port dimensions and suggestions without specific recommendations [21]. Tumwesige et al. summarized how off-the-shelf biogas burners compared to a newly developed burner with three millimeter circular ports [5]. Most recently and with the most relevance to the study described in this paper was conducted by Jadhav et al. in 2015. Their group conducted a computational fluid dynamics and genetic algorithm model to determine optimal circular port diameter and distribution, arriving at a recommended burner head with 30 circular ports at 4 mm each [22]. This published study did not indicate experimental validation of the results.

1.6 Biogas Burner Development

Biogas burner development began in the late 1970's under the Development and Consulting Services of the United Mission to Nepal [23]. Since then, researchers across the world have recognized the growing need for the development of biogas specific burners. In response, there have been a number of journal articles and reports published to help educate and inform the space. In 1991, Chandra and colleagues at the Indian Institute of Technology in New Delhi developed a mathematical model to describe the dynamics behind the entrainment effect and experimented with flame quenching due to the distance between the burner head and the pot [24], [25]. In 1996 and 2014, Fulford and colleagues created an overall biogas burner design guide and reviewed biogas stoves in Uganda, asserting that local stove quality and performance do not match

Chinese and Indian standards [9], [21]. In 2009, The Netherlands Development Organization (SNV) commissioned stove testing from regions in Africa and Southeast Asia arriving at similar conclusions [26]. In 2015, Jadhav et al. conducted flame port design simulations as discussed in Section 1.5.1 [22] Other studies by Itodo et al., Obada et al. and Kurchania et al. developed entire burner assemblies as part of their work [27]–[29]. Although there have been recent research efforts, domestic biogas burner literature has yet to reach the granularity that is presented in the LPG and natural gas cooking appliance literature.

Due to the work of government and international organizations as well as the implementation of Chinese and Indian biogas regulations, there are several appropriately designed burners available in different regions around the globe. Puxin in China, Rupak in India, Montals in Ghana and the Development Technology Workshop in Cambodia represent a few organizations that provide a biogas burner. An alternative option is the modification of an off the shelf LPG burner through the expansion of the injector orifice and flame ports appropriately.

The design of biogas burners is similar to the concepts of LPG burner design with the fundamental differences of stoichiometric air requirement, energy content and supply pressure. Biogas has a lower calorific value than LPG and thus requires less air per unit of fuel for complete combustion. Domestic biogas is supplied through small scale biodigesters and rarely have supplementary compression mechanisms to reduce gas volume for long term storage. Therefore, gas pressure will vary throughout a cooking event. So, without the modification of the LPG injector orifices and flame ports, the higher pressure drop through conventionally smaller LPG orifices and ports will likely reduce overall efficiency and may prevent continuous stove operation. A study by Ko and Lin compliment this discussion by asserting that using the same gas stove design to burn gases with various heating values is inappropriate and hazardous [30].

1.7 Research Summary and Hypotheses

In response to the design challenges described in the literature, this research aims to utilize a combined design, modeling and experimental approach to improve biogas combustion performance in household burners (Figure 5). To reach this goal, a framework and tool were developed that others can follow to evaluate burner combustion. The study began with an experimental validation of the composition of biogas to inform computational models and laboratory experiments. After consideration of literature design suggestions and initial experimental results of off the shelf burners, flame port designs were translated into 3-D SolidWorks® renderings. The 3-D renderings were subject to simulation in ANSYS® Fluent and Chemkin® for combustion performance calculation, adopting similar methods as previous researchers [22], [31], [32]. The highest ranked designs were manufactured using Direct Metal Laser Sintering (DMLS) and their performance measured in laboratory experiments. This approach considered a series of burner flame port designs specific to one biogas burner (called the *Lotus*) and tested the validity of the following hypotheses.

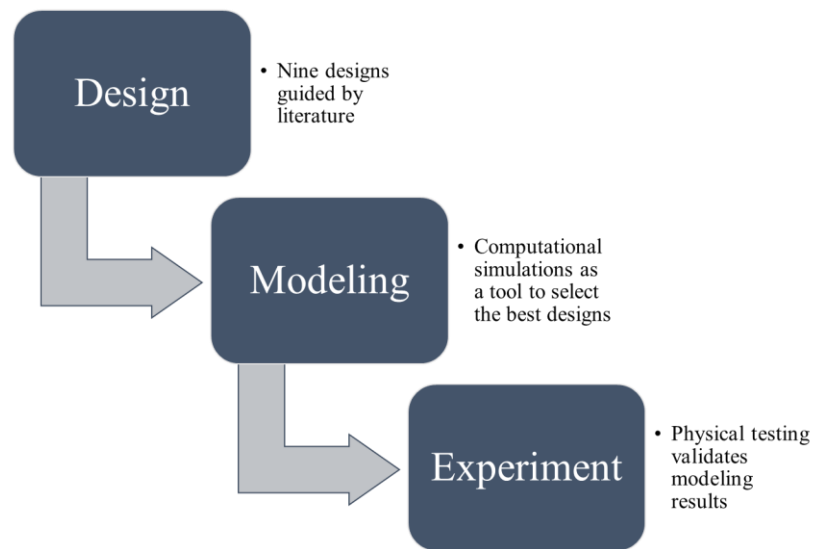


Figure 5 – Approach concept combining design, modeling and experiments

1. Modern engineering software tools can accurately and effectively guide biogas burner flame port design.
2. By making analysis-driven alterations to the shape, spacing and configuration of burner flame ports, the thermal and combustion efficiency of biogas burners can be improved.

CHAPTER 2. DESIGN AND MODELING METHODS

2.1 Flame Port Design

The Lotus biogas burner, designed and manufactured by the Development Technology Workshop in Cambodia, is a partially premixed burner design funded by the Netherlands Development Organization (SNV). The burner is comprised of a modular upper cap with a flame port assembly that fits well into the aims of this study. Given the built-in modularity and history of development with SNV, the Lotus burner was chosen for this research to test both stated hypotheses.

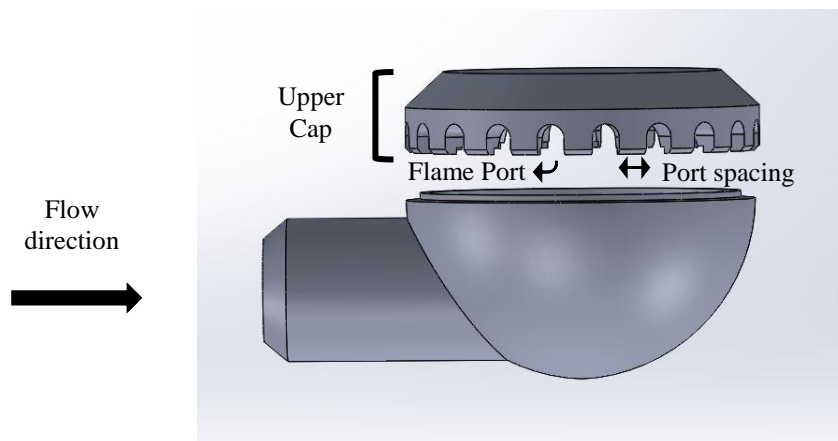


Figure 6 – Original Lotus biogas burner flame port design

Setting the original burner flame port configuration as the baseline (Figure 6), nine designs were developed that considered recommendations made by Jones, Fulford, Tumwesige et al., and Jadhav et al. [9], [14], [21], [22] (Table 2). Such recommendations included the use of four (4) mm circular ports, a lower than six (6) mm inter-port spacing, a port depth to diameter ratio greater than two (2) and a greater than four (4) to one (1) ratio of length to width for rectangular ports. Other burner components including the mixing tube, injector orifice and total port area were not varied.

This study focused on flame port geometry in an attempt to isolate the influence of changes to flame port spacing, shape and configuration on combustion performance. The nine designs were chosen by combining values that exceeded, met and were lower than the recommended or optimal factors as suggested by the literature while keeping total port area constant across each design. This design selection method was intended to test the validity of the suggestions in literature and to combine geometries not yet evaluated in previous biogas burner studies. Designs 1a, 1b and 1c were created to test the effect of decreasing the ratio of depth to diameter (1.65 to 1.1) and increasing port spacing (1.95 to 4.30 mm). Designs 2a, 2b and 2c were created to test the effect of increasing length to width ratio (2 to 6) while decreasing port spacing (7.90 to 2.60 mm). Designs 3a, 3b and 3c were created using a combination of circular and rectangular geometries.

Table 2 – Flame port design dimensions and descriptions

Design	No. of Ports	Circular Port Diameter (mm)	Rectangular Port Length and Width (mm)	Port Spacing (mm)	Port Geometry
Original	20	5.5	-	5.80	D-shaped
1a	48	4	-	1.95	Circular
1b	32	5	-	2.30	Circular
1c	22	6	-	4.30	Circular
2a	19	-	8 (L) 4 (W)	7.90	Rectangular
2b	38	-	8 (L) 2 (W)	3.90	Rectangular
2c	58	-	8 (L) 1.3 (W)	2.60	Rectangular
3a	28	14 x 4	14 x 8 (L) 4 (W)	2.08	Circular & Rectangular
3b	34	17 x 4	17 x 8 (L), 3 (W)	3.14	Circular & Rectangular
3c	54	27 x 3	27 x 8 (L), 2 (W)	1.68	Circular & Rectangular

2.2 Biogas Composition

2.2.1 Laboratory Evaluation

An experiment was conducted at the Powerhouse Energy Campus in Fort Collins, Colorado to understand the realistic biogas properties as generated in a decentralized biodigester. The average biogas properties measured in this experiment were used as input values for the computational simulations and experimental trials.



Figure 7 – Mobile biodigester experiment

The experiment was completed using a Sistema Biobolsa 2.3 cubic meter tubular biodigester housed in a custom, above ground mobile platform (Figure 7). The biogas generation process was initiated by adding roughly 0.5 cubic meters of water mixed with 0.13 cubic meters of ruminant (cow) manure. Anaerobic micro-organisms naturally occur in cow manure and once a healthy colony populates a biodigester, a regular supply of biogas can be generated through a mesophilic process. For this study, the initial slurry loading was left to incubate for three weeks, after which a weekly loading schedule of 15 gallons of manure and 45 gallons of water was implemented.

At the fifth week of the weekly loadings, a sample of biogas was drawn from the digester for composition analysis. A flammability test determined five weeks to be enough time to allow

for the stabilization of the micro-organism population and in turn production of flammable biogas. The sample was drawn through a sampling rig from the biogas supply line after a hydrogen sulfide scrubber. The sampling rig was comprised of a diaphragm pump connected to a sealed gas sample bag (Figure 8).

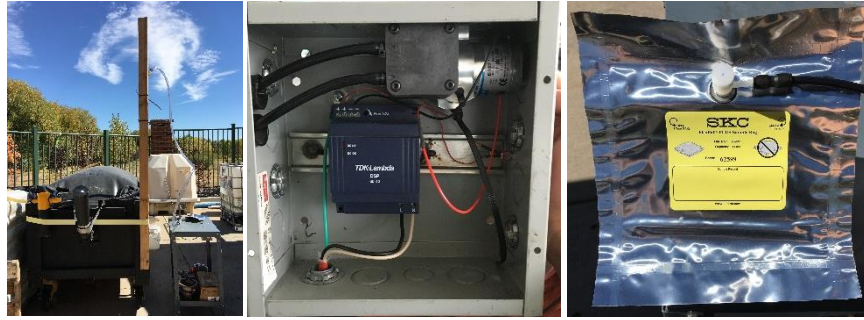


Figure 8 – Gas sampling set up, pump and sealed sample bag

The sampled gas was analyzed through gas chromatography via a third-party vendor. Gas chromatography is a process that vaporizes a sample and separates the different compounds of that sample for identification. The results provided an average value near 60 mole percent methane, 40 mole percent carbon dioxide and 130 ppm hydrogen sulfide, falling into the expected composition range stated in literature (Table 3) [8].

Table 3 – Laboratory biogas composition results

Component	Test 1	Test 2	Average
CH₄ mol %	64.28	59.19	61.74
CO₂ mol %	35.72	40.81	38.26
H₂S ppm	263.0	5.40	134.2

Therefore, a 60 mole percent methane and 40 mole percent carbon dioxide blend was used as the benchmark gas throughout the rest of the study. Hydrogen sulfide was excluded from this study to limit modeling complexity and equipment corrosion in the laboratory.

2.2.2 Field Evaluation

Real time field sampling of biogas composition was conducted in the state of Gujarat, India. The gas from six active tubular, one fixed concrete dome and one HDPE floating dome biodigesters were sampled using a LANDTEC® Biogas 5000 Portable infrared and electrochemical analyzer (Figure 9). The field results in Table 4 were collected after the conclusion of the study and fall below the 60 mole percent utilized, but remain within the 50-70 mole percent listed in literature. Future field evaluations beyond India are needed to confirm these findings.



Figure 9 – Biogas 5000 portable infrared and electrochemical analyzer

Table 4 – Results of the field evaluation of biogas composition in Gujarat, India

Type	Age	CH4 %	CO2 %	Balance %	H2S ppm
Tubular	2 months	52.1	42.6	5.0	266
Concrete Fixed Dome	10 years	52.9	43.9	3.0	149
HDPE Floating Dome	2 months	48.1	48.0	3.7	110

2.3 Modeling

To simulate biogas combustion with the various flame port designs, a modeling tool was developed using SolidWorks®, ANSYS® and Chemkin®. ANSYS® models flows and reactions based on the Navier-Stokes equations and Chemkin® solves reaction problems and produces detailed combustion parameters. The tool has two parts: the first to simulate fluid mixing profiles, and the second to simulate combustion of the gas. The objective of the model was to identify the three highest performing burner geometry configurations compared to the original Lotus design. Performance rankings were determined by simulated maximum flame and average zone temperatures and emissions of carbon monoxide, carbon dioxide and unburned methane.

To use the tool, fuel properties were defined and two 3-D renderings were created in SolidWorks®: a complete burner assembly, as well as flame ports attached to an external volume. By inserting the burner assembly, fuel composition and an initial flow rate into the ANSYS® computational fluid dynamics (CFD) mixing model, the flow rate of entrained air and exit flow velocities were calculated. In parallel, a lookup table of equivalence ratio versus laminar flame speed was created in Chemkin® using the same fuel composition. The lookup table enabled the comparison of exit flow velocities to laminar flame speed via the equivalence ratio generated in the CFD mixing model.

The output of the mixing model using 170 liters per hour was entered into the ANSYS® flame port combustion model. This model produced flame and zone temperatures as well as emissions species that were used in an equally weighted ranking procedure to select the three highest performing designs.

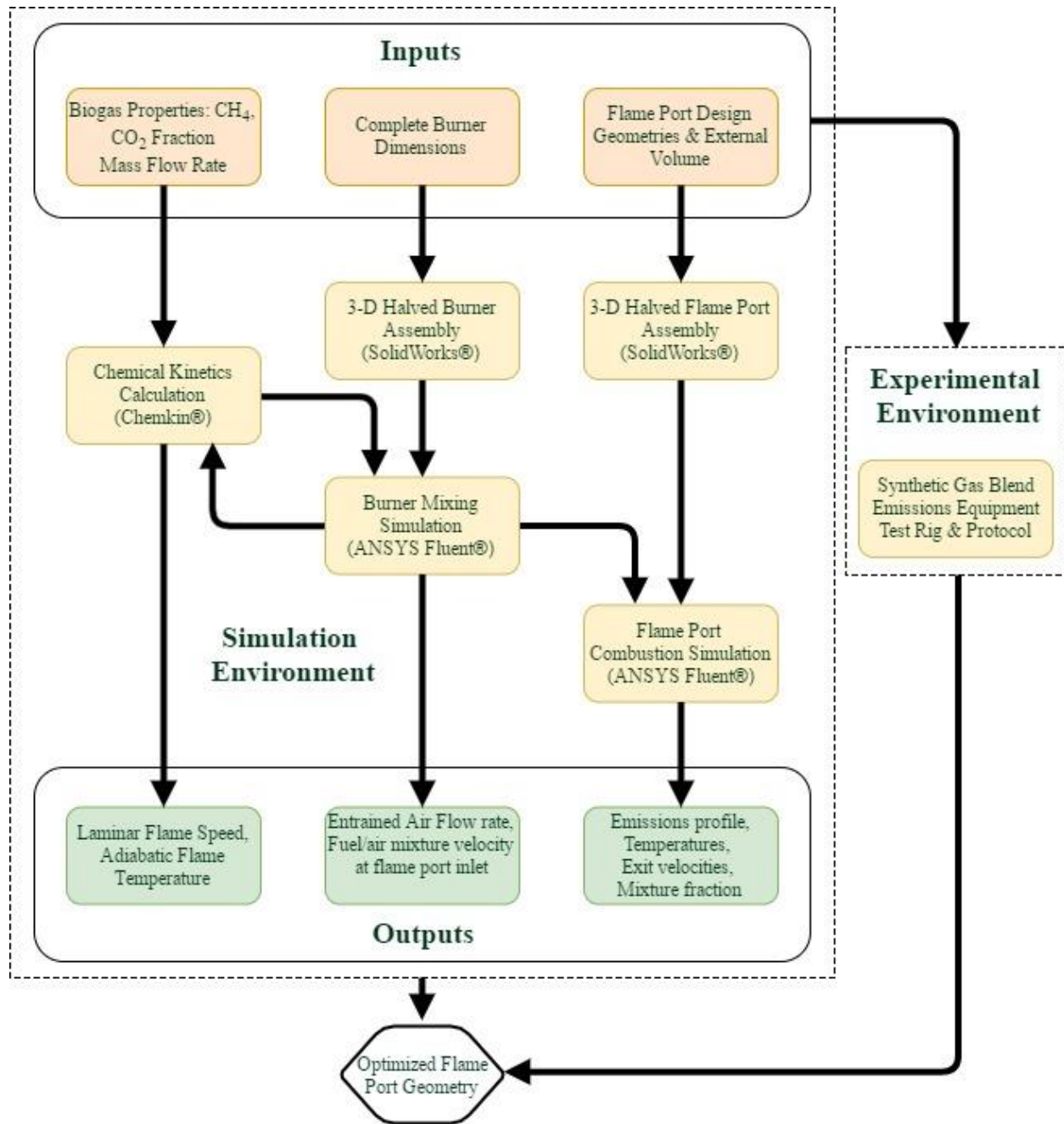


Figure 10 – Process flow diagram of the modeling tool.

The utilization of modern software tools sought to enable rapid design iteration and optimization without the investment of manufacturing. Although not entirely representative of physical conditions and results, the models were constructed and operated to mimic the experimental validation environment.

2.3.1 3-D Assemblies

A series of to-scale 3-D SolidWorks® models of the entire Lotus burner assembly were created to anchor the computational models (Figure 11). As represented in Figure 6, the base model was constructed in a modular fashion to allow for the substitution of flame port designs detailed in Table 2. In order to have a path for gas to flow through the burner, the rendering needed to be filled and peeled back. The ensuing renderings were halved in a symmetrical fashion to reduce modeling time (Figure 11). These renderings were used as the 3-D model for the first component of the computational simulation to determine fuel mixture flow rates and velocity values immediately before ignition.

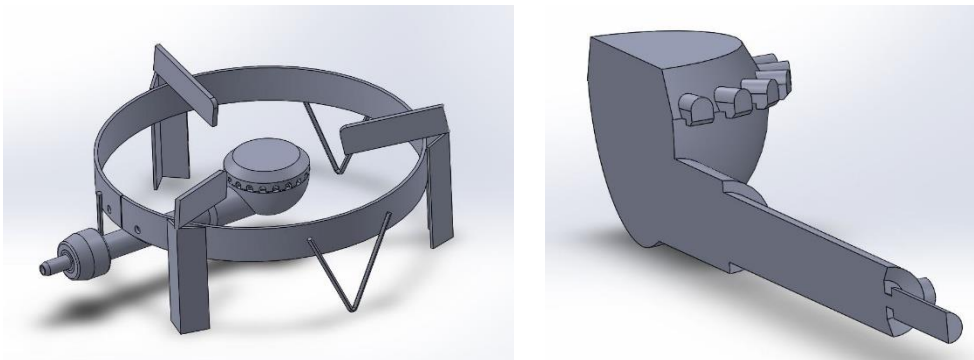


Figure 11 – Lotus burner assembly, complete and halved

A second series of 3-D SolidWorks® models were constructed and halved symmetrically to solely represent the flow and ignition of a fuel mixture from the cavity of a flame port to a fixed external volume (Figure 12). These renderings were used as the 3-D models for the second and final component of the computational simulation. This second series of 3-D renderings provided the foundation to produce combustion performance predictors for design evaluation.

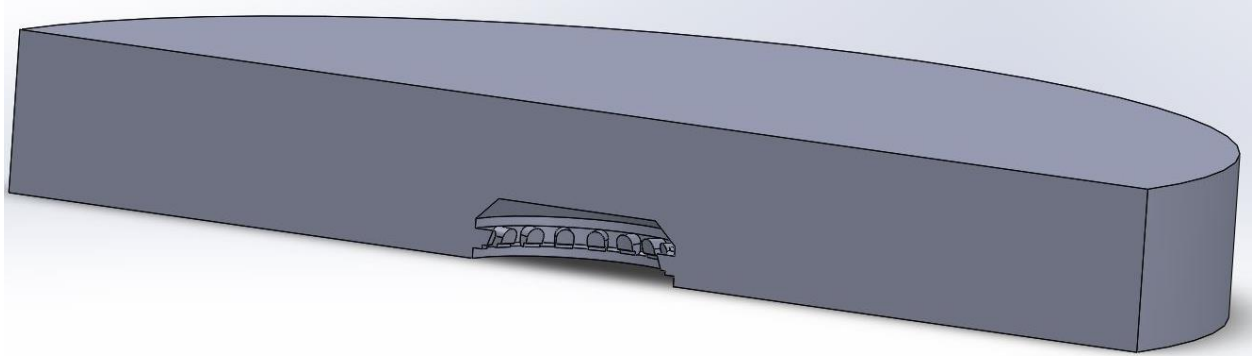


Figure 12 – Flame ports and external volume model

2.3.2 Chemical Kinetics Calculations

Chemical kinetics inform the time required for a given reaction(s) to occur and are a function of temperature, pressure, oxidizer, fuel quantity and fuel type. The chemistry for this study, in both the computational and experimental environments, was based around partially premixed combustion. Within the Lotus burner, ambient air is entrained into the mixing tube due to a pressure gradient following the injector, leading to partially premixed combustion. To understand the influence of chemical variables, such as the amount of entrained air and biogas methane fraction, on biogas combustion, the software tool Chemkin® was used. For this study, the Gas Research Institute (GRI) 3.0 chemical reaction mechanism was used with Chemkin® to evaluate laminar flame speed and adiabatic flame temperature by varying methane fraction and equivalence ratio [33]. Standard temperature (20°C) and pressure (101 kPa) were used in the model.

Laminar flame speed (S_L) is defined as the velocity at which unburned gases move through the combustion wave in the direction normal to the wave surface [11].

$$S_L = \sqrt{\text{Thermal Diffusivity}(\alpha) * \text{Reaction Rate}}$$

Adiabatic flame temperature is defined as the highest temperature that can be achieved given a set of reactants without heat transfer to the environment. Adiabatic temperatures provide an upper threshold, but heat losses to the physical environment limit a flame's temperature in practice.

Due to fluctuating environmental and feedstock conditions in an anaerobic digester, the methane concentration in biogas can vary over a period of time. Within the Chemkin® simulations, the methane concentration in biogas was varied between 20 % and 100 % at intervals of 20%.

Within a biogas burner, the air entrained into a mixing tube can also vary significantly. This variable is represented by phi, or the equivalence ratio (Φ). In this study, equivalence ratio is defined by the stoichiometric air to fuel ratio divided by the actual air to fuel ratio on a mass basis. Within the Chemkin® simulations, phi was toggled from 0.5 to 1.5 at intervals of 0.1. The highest laminar flame speed occurs at the stoichiometric mixture front, where phi equals one.

$$\varphi = \frac{\frac{A}{F} \text{ stoichiometric}}{\frac{A}{F} \text{ actual}}$$

The results from the 60 mole percent methane Chemkin® case were used as benchmark values for phi, laminar flame speed and flame temperature comparison. A lookup table was created with results in Figure 13 by toggling phi to produce a corresponding laminar flame speed and adiabatic flame temperature of the burner (lookup table is in Appendix A). The only laminar flame speed used for reference in this study was the highest value for the 60 mole percent methane case (25.3 cm/s), occurring at the stoichiometric mixture front of each flame. The flame speed decreases in both the fuel rich (phi greater than one) and fuel lean (phi less than one) regions of the flame. Fuel rich regions in this study are below the stoichiometric mixture front and fuel lean regions are above the front.

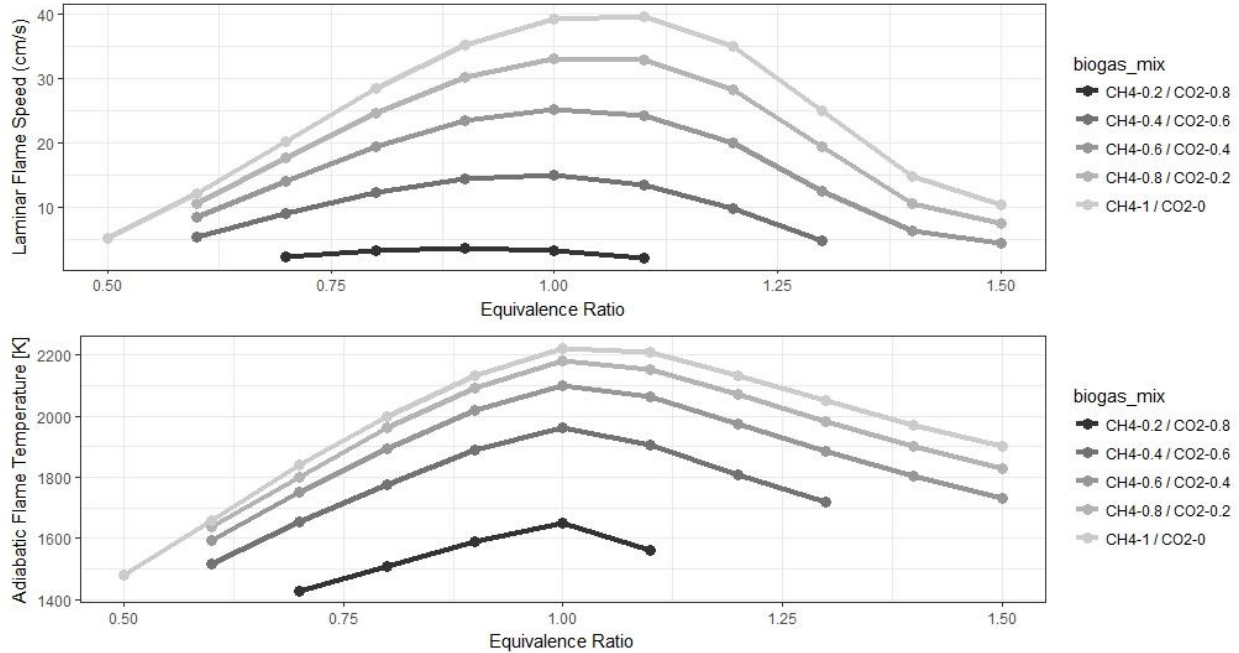


Figure 13 – Adiabatic flame temperature and laminar flame speed were modeled in Chemkin as a function of equivalence ratio. (Produced using the GRI 3.0 Mechanism)

2.3.3 Computational Fluid Dynamics Simulation

2.3.3.1 Burner Assembly Mixing Simulation

The first part of the ANSYS Fluent® simulation contained the halved burner configuration (Figure 11) and did not include combustion. The simulation comprised of species transport (GRI 3.0), energy equation and viscous k-epsilon (realizable) models. The simulation boundary conditions were defined by a pressure inlet for entrained air, a velocity inlet for biogas, a pressure outlet at the flame port exits, symmetry on the halved surface and a wall boundary for the remaining surfaces.

The pressure inlet for entrained air was set to require air species as 79 percent nitrogen and 21 percent oxygen. Other trace gases in ambient air were ignored. The fuel inlet for biogas entry into the burner was set to 1.23 m/s (lowest flow rate for a self-maintaining flame) with mole fractions of 0.6 methane and 0.4 carbon dioxide. The pressure outlet at the flame ports was specified to contain an initial guess of mass fractions of four species as defined in Table 5. The

values in Table 5 were calculated based on the expected amount of air entrained at the user-defined mass flow rate.

Table 5 – Pressure outlet initial mass fraction guesses

Species	Mass Fraction
Methane (CH ₄)	0.1156
Carbon Dioxide (CO ₂)	0.2114
Nitrogen (N ₂)	0.5162
Oxygen (O ₂)	0.1568

After 2,000 iterations run at double precision in parallel, the simulation produced fuel mixture velocity profiles throughout the burner, values of flow rate of entrained air as well as biogas and entrained air homogeneity. With the produced equivalence ratio and the set inlet boundary condition, manual calculations were performed to confirm the predictions of the simulation (Appendix A.). The manually calculated velocity and mixture density values following the procedure listed in Appendix A. were used to determine Reynolds number.

2.3.3.2 Flame Port Combustion Simulation

The second and final part of the ANSYS Fluent® simulation isolated the flame ports for biogas combustion evaluation. This simulation consisted of non-premixed combustion species (inlet diffusion, GRI 3.0), P1 radiation, viscous k-epsilon (realizable) and energy equation models. Within the species model, the fuel stream rich flammability limit was set at 0.6 (as determined for biogas), the GRI 3.0 mechanism thermodynamic file was uploaded and the boundary tab was filled with the values in Table 6.

Table 6 – Boundary tab species mass fraction of species in air

Species	Fuel	Oxidizer
CH ₄	Output from CFD Part 1	0
N ₂	Output from CFD Part 1	0.767
O ₂	Output from CFD Part 1	0.233
CO ₂	Output from CFD Part 1	0

Once applying the values in Table 6, a PDF table was calculated under the Boundary tab of the species model and applied. The PDF table was exported to the default file location.

The simulation boundary conditions were defined by a velocity inlet at the flame ports and a pressure outlet at the boundary of an external volume. A symmetry boundary was applied to the halved surface and a wall boundary to all other external surfaces. The velocity inlet was set to the average outlet velocity as calculated in the part one simulation and the fuel mean mixture fraction was set to one. To facilitate an uninterrupted simulation, the under-relaxation factor, P1, was changed from the default of one to 0.9. The simulation was run through 4,000 iterations at double precision in parallel to produce flow velocities, temperatures and exhaust speciation as a result of combustion. The exhaust species of interest were carbon monoxide, carbon dioxide and methane. Sulfur oxides and water vapor were excluded due to their limited concentration in biogas. Nitrous oxides were excluded due to an inability to reach a nitrogen mass balance in the combustion simulation. This was a result of a limited computational area to reduce required processing power.

2.3.4 Port Design Rank

Each of the ten port designs, nine developed in this study and the original, were compared against each other for selection. The designs were compared using the results from ANSYS® flame port simulation. Specifically, maximum temperature, average zone temperature, unburned methane flow rate and combustion efficiency were used as predictors for comparison of the design as a factor. Modified combustion efficiency was calculated from the carbon monoxide and carbon dioxide flow rates generated by the model [34].

$$\eta_{\text{combustion}} = \frac{[CO_2]}{[CO_2] + [CO]} \times 100$$

The four predictors used for comparison were equally weighted via a simplified version of the simultaneous optimization technique developed by Derringer and Suich [35]. Weighting the predictors when ranking can be possible in other applications when the influence of a certain predictor is proven to be more important than another. The designs that achieved the highest temperatures, highest combustion efficiency and lowest unburned methane flow received a rank of one in that category. The designs received a rank for each predictor and the ranks were totaled. The three designs that had the lowest total were selected for manufacture.

$$\text{Total Rank}_{\text{model}} = T_{\text{zone [K], rank}} + T_{\text{max [K], rank}} + \text{Unburned CH}_4, \text{rank} + \eta_{\text{combustion, rank}}$$

CHAPTER 3. EXPERIMENT SETUP AND METHODS

3.1 Experiment Overview

The experimental portion's objective was to validate the results of the modeling tool and gain flame port design insight from off the shelf burner testing. The characteristics of cookstoves contribute to highly variable and interdependent combustion and heat transfer, which makes modeling these processes difficult and uncertain [36], [37]. Therefore, physical testing was conducted to validate the products of the modeling design tool. The three selected designs were manufactured via Direct Metal Laser Sintering (DMLS) and assembled in conjunction with the remaining pieces of the burner for testing. The data recorded in the experiment included CO, CO₂ and CH₄ emissions and thermal efficiency derived from ten minute tests where biogas was applied to the experiment at the same flow rate as to the modeling tool. Each test was started with the burner at ambient conditions. Supplemental tests were conducted in parallel to understand cause and effect relationships among several burners.

3.2 Experiment Setup

3.2.1 Biogas Supply

Challenges emerge when conducting a validation experiment with biogas from an anaerobic digester. Variable environmental conditions and feedstock composition occur daily, leading to changes in the methane concentration, and thus energy content, of biogas. Chae et. al. proved that with a drop in 10 °C, methane yield was reduced by near 18% [38]. Therefore, tests on multiple days may be conducted with biogas that has a range of energy contents. Another variable is biogas supply pressure. The pressure of biogas within a digester builds as gas is produced. Gas production in a digester is often outcompeted by the gas consumption of an appliance and thus the gas supply pressure decreases over the use period. Even if methane content

and pressure do not vary, accurately measuring the mass flow rate of biogas consumption from a biodigester requires a high precision and high cost instrument.

To reduce the number of variables presented by biogas supplied from a biodigester, cylinders of a synthetic biogas blend were used for this study (Figure 14). The blend was comprised of 60 mole percent methane and 40 mole percent carbon dioxide as determined from the tubular biodigester experiment and gas chromatography results. The amount of blended gas that can fit in a cylinder is limited by the pressure of carbon dioxide. If the partial pressure of the carbon dioxide component is set too high, the gas will condense to a liquid and there will no longer be a homogenous gas mixture. The initial gas cylinder pressure for this work was approximately 1200 psi.



Figure 14 – Synthetic 60 mole % methane, 40 mole % carbon dioxide biogas blend in a pressurized cylinder

The cylinder from the third-party vendor included the pre-blended gas, cylinder and stock cylinder gate valve. Since the gas was majority methane, a Compressed Gas Association (CGA) 350 fitting was required to connect the gate valve to a cylinder regulator. The cylinder regulator was a two-stage high pressure regulator designed for hydrocarbon gases. Immediately downstream of the regulator a flashback arrestor was installed. The flashback arrestor contained a check valve and sintered element to prevent reverse flow and to quench any flames that may travel toward the tank.

3.2.2 Biogas Flow Control

The experiment set the mass flow rate to 0.052 grams per second, or the flow rate that correlates to the inlet velocity set in the modeling design tool (1.23 m/s).

$$\dot{m} \left[\frac{kg}{s} \right] = \rho_{biogas} \left[\frac{kg}{m^3} \right] * v \left[\frac{m}{s} \right] * A_{inlet} [m^2]$$

$$\rho_{biogas} \left[\frac{kg}{m^3} \right] = \frac{P [Pa] * MW_{biogas} \left[\frac{kg}{kmol} \right]}{R \left[\frac{J}{kmolK} \right] * T [K]}$$

The mass flow rate was controlled and locked in at the set point through an iterative process. The difference in mass of the gas cylinder over a period of time was recorded and a mass flow rate was calculated. To hone in on 0.053 grams per second, the gate valve on the inlet regulator (Figure 15) was adjusted in a stepwise fashion while monitoring the change in mass of the cylinder over a set period of time. An improved yet more costly method would be to purchase and calibrate an ALICAT Scientific® mass flow controller that can automate the process of setting and monitoring the mass flow rate.



Figure 15 – Combined with a cylinder scale, the regulator provides flow control adjustment while the Magnehelic gauges provide supply pressure monitoring

3.2.3 Sampling Equipment

The Advanced Biomass Combustion Laboratory at Colorado State University has established a robust suite of tools and instruments that allow for scientific collection of experimental data. This study leveraged the resources available to achieve the desired objectives of validating the modeling design tool (Table 7).

Table 7 – Equipment and instruments to complete the experiment

Description	Manufacturer & Model	Function Comments
Laminar flow hood	NA: custom built	Safe and controlled capture of flue gases
Thermocouple array	Omega® K-type thermocouples	Various gas, stove and chimney temperatures
Particulate matter (PM) sampling	2.5µm & 10µm URG Corp Cyclones	Custom filter collection of particulates
PM sampling control	Alicat® mass flow controllers	Flow control based on ambient pressure and system temperatures
Inlet Regulator	Equilibar Model 10212-Z22435	Inlet flow control
Cylinder Regulator	Airgas Y12-D244D	Gas cylinder pressure reduction
Micro Balance	Mettler Toledo - 1µg Precision	Filter mass recording
Large mass scale	Adam Equipment GFK 330aH	Measure of the cylinder change in mass
Small mass scale	Adam Equipment GBK 35a	Measure of the pot and water used in a test
7-liter stainless steel pot	Common cooking appliance	Contains water throughout a test
Flashback arrestor	Superflash EDI-0004	Prevents flashback to the cylinder
Synthetic Gas Blend	Airgas 60 mol% CH ₄ 40 mol% CO ₂	Gas in a pressurized cylinder made to represent biogas
Pressure gauge	Magnehelic 0 - 15 " H ₂ O	Measures supply pressure to the burner
Non-Dispersive Infrared Spectrometers	Siemens Ultramat 6	Real time CO, CO ₂ and Hydrocarbon concentrations

3.2.3.1 Laminar Flow Hood

To effectively capture the entire emissions stream from a biogas burner, all data was collected within an enclosed hood. The emissions stream in the hood was drawn into a collection and analysis system via a fixed pump set to 6011 liters per minute (1340 RPM) (Figure 16). The hood directs flow into a particulate matter sampler and a non-dispersive infrared analyzer. The hood is equipped with temperature, pressure and mass flow control which is managed via a central

program. The influence of an induced draft created by the pump in the hood is mitigated by collecting baseline data before each test.

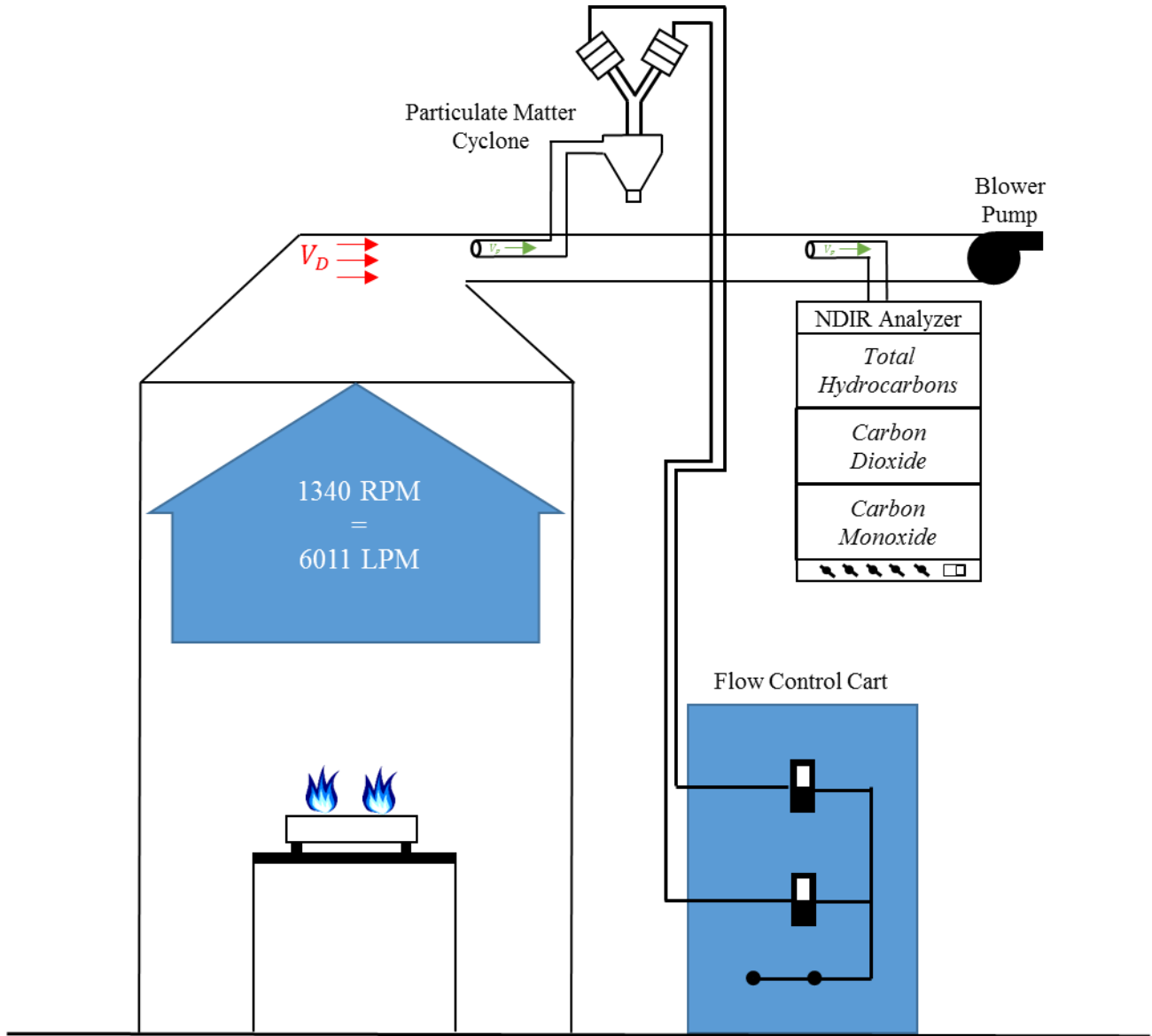


Figure 16 – Diagram of the flow hood, particulate matter control and collection system and the gaseous emissions NDIR analyzer

3.2.3.2 Supervisory Control and Data Acquisition (SCADA)

Experiment monitoring, recording and control was managed through several custom-built National Instruments LabVIEW® software programs. Figure 17 displays the three separate

programs that manage water temperature and pump speed, gas temperature and pressure compensation and gaseous emissions analysis.

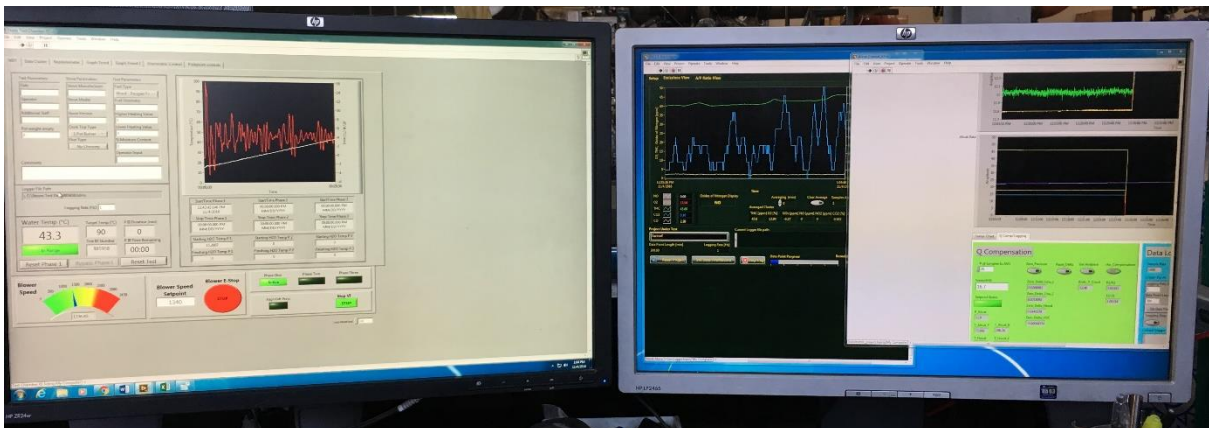


Figure 17 – Far left: Manages pump speed and water temperature, Middle: Manages NDIR results, Far right: Manages temperature and pressure compensation

3.2.3.3 Gaseous Emissions

The gaseous emissions produced from biogas combustion were measured by a suite of non-dispersive infrared (NDIR) sensors through heated sampling lines. Before each day of testing the NDIR sensors were user calibrated with set calibration gases. The compounds of interest were methane (CH_4), carbon monoxide (CO) and carbon dioxide (CO_2). Methane and carbon monoxide data were presented in units of parts per million (ppm), and carbon dioxide data was presented in units of percent. The NDIR sensors measure total hydrocarbons, but methane is the only hydrocarbon present in biogas in noteworthy quantities. The following steps detail the process of how the gas compounds were measured and converted to a uniform mass flow.

1. Before the beginning of each test, a five-minute background was recorded for all three compounds of interest.
2. Hood temperature and pressure was recorded to calculate air density. The total hood mass flow was calculated from both the density and the fixed volumetric flow rate of the pump.

3. A test was started and concentrations (ppm and %) of the three gas compounds were recorded by the NDIR analyzer.
4. At the conclusion of the test, the background values of each compound were subtracted from the values recorded and CH₄ and CO values were converted from ppm to %.
5. Using the density and total mass flow of gas in the hood and the density of the specific gas compound, a mass flow per sampling increment (one second) was calculated for each compound.

3.2.3.4 Particulate Matter Emissions

Particulate matter (PM), or black carbon, is emitted as a result of incomplete combustion of a carbonaceous fuel. Compared to improved biomass cookstoves, gaseous fuel cookstove PM emissions are negligible [39]. This study conducted several PM measurements throughout the duration of a test confirming that PM was below the detection limit for the Lotus biogas burner.

The custom particulate matter sampling equipment detailed in Figure 15 and Table 7 was used with PALLFLEX® punch membrane filters (Figure 18). The filters were created using a punch and were equilibrated in a temperature and humidity controlled environment for 24 hours pre-test and for 12 hours post-test.

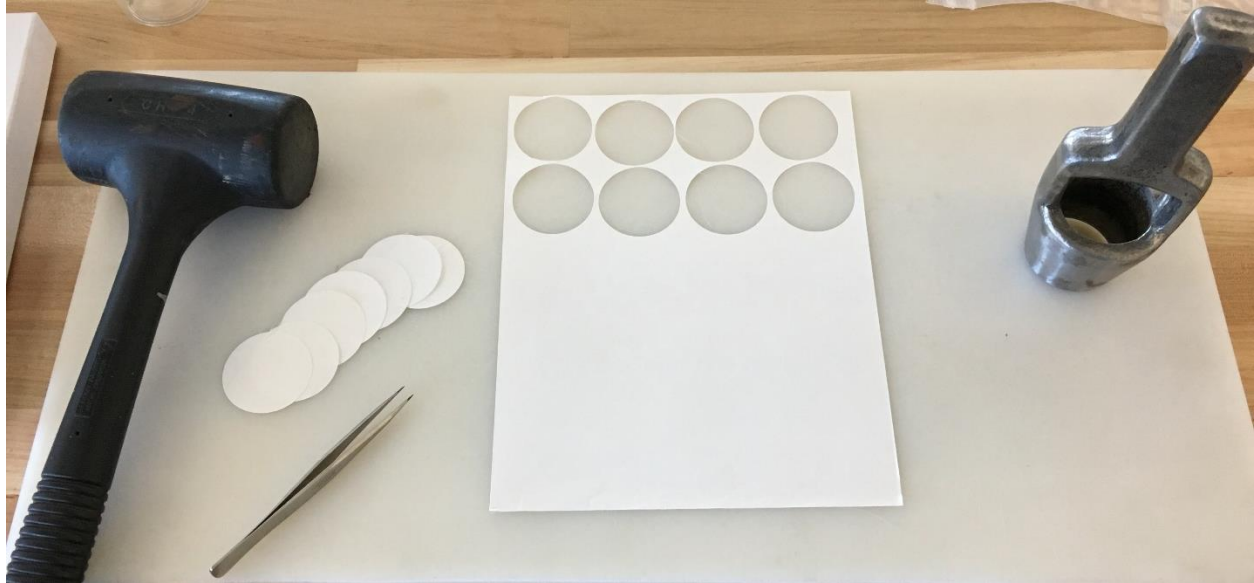


Figure 18 – PALL filters were created and equilibrated to measure particulate matter emissions from biogas burners

The following list details the procedure of particulate matter sampling. This procedure was conducted for nine tests with varying conditions. For particulate matter samples to be considered accurate and relevant, they need to abide by the definitions of the limit of detection (LOD) and limit of quantification (LOQ) relative to filter blanks. The LOD is equal to the average mass accumulated on the filter blanks plus 3 multiplied by the sample standard deviation. The LOQ is equal to the average mass accumulated on the filter blanks plus 10 multiplied by the sample standard deviation.

$$LOD = \overline{\Delta m_{blank}} + 3s$$

$$LOQ = \overline{\Delta m_{blank}} + 10s$$

If a measurement was below the LOD, a test cannot be certain that any mass was collected on a filter. If a measurement was above the LOD, but below the LOQ, a test can be certain that mass was collected on a filter but not exactly how much mass was collected.

1. The mass of the filters was recorded on an ultra-sensitive scale (1 microgram) and transported to the sampling equipment in a sealed container.
2. A filter blank was added to the sampling equipment and removed to test filter mass change as a result of adding and removing the filter to the equipment
3. A filter background was conducted for 30 minutes for each day of testing to determine the particulate loading in the ambient air.
4. The sampling equipment pumps were turned on and a new filter was added for each test conducted.
5. After the post-test equilibration period, the mass of each filter was recorded on an ultra-sensitive scale (1 microgram).

3.2.4 Design Manufacturing

The three selected flame port geometry designs for the Lotus biogas burner using the modeling tool were manufactured for tool validation. The SolidWorks® renderings were converted to a 2-D design specifications sheet that included dimensions and tolerances (Figure 19).

3.2.5 Testing Protocol

The experiments conducted to validate the modeling tool followed a combination of the International Workshop Agreement (IWA) water boiling test (WBT) protocol and a Colorado State University developed firepower sweep protocol [41], [42]. Specifically, a five-liter cold start test was used as the structure for the experiment. The test is termed cold start, because the entire stove is at ambient temperature before the beginning of the test. The IWA WBT protocol calls for temperature controlled tests, or the duration of a test set by the time required to raise the temperature of five-liters of water from 15°C to boiling, or 90°C.

Rather than perform the standard temperature controlled tests, an initial series of time controlled ten-minute cold start tests were conducted starting with 5L of water at 15°C using the same conditions as set in the modeling tool (biogas mass flow rate of 0.052 grams per second). This defined flow rate was termed a low firepower condition. Shorter, time controlled tests are possible with gaseous burners due to a constant, linear change in water temperature over time (Figure 21). In contrast, biomass (wood) cookstoves have shown gradual changes to the slope of temperature versus time over the duration of a test with greater noise as compared to gas burners.

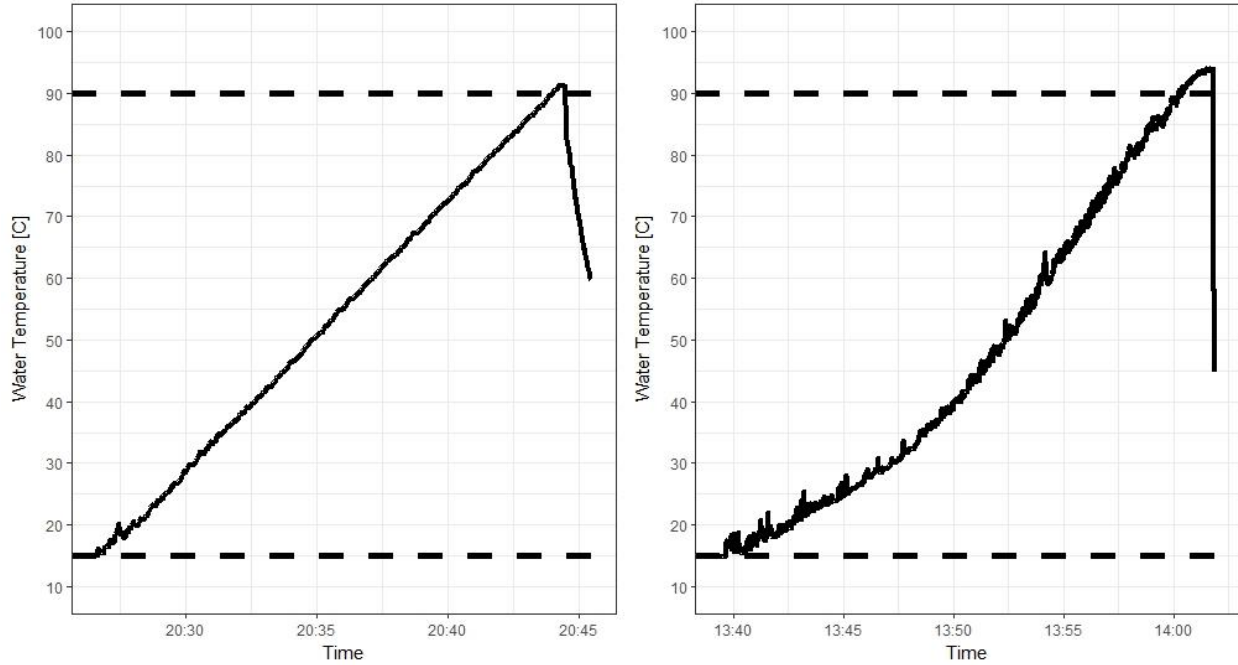


Figure 21 – Left: Gas fired water boil test, Right: Wood fired water boil test

The three selected flame port geometry designs as well as the original design (four total) were repeatedly tested at the low firepower condition to establish a level of confidence in the results. Studies by Wang et al. and L’Orange et al. were considered when deciding the number of repetitive tests to be conducted [43], [44]. The metrics for evaluation of each experimental test included thermal efficiency, modified combustion efficiency (for eqn. see Section 2.3.4), grams of carbon monoxide per mega joule of energy delivered and grams of unburned methane. Thermal efficiency was defined as the energy delivered to a 5L pot of water divided by the total energy provided to the burner in the form of fuel. Thermal efficiency was a function of flame temperature and structure, pot dimensions and distance from the burner to the pot. In this experiment, pot dimensions and distance from the burner to the pot was fixed.

$$\eta_{\text{thermal}} = \frac{(\text{mass}_{5L \text{ of water}} * C_{p,H2O} * \Delta T) + (\Delta \text{mass}_{H2O} * h_{e,H2O})}{\text{fuel consumed [kg]} * \text{Calorific Value} \left[\frac{J}{kg} \right]}$$

The following steps outline the protocol for each test.

1. The mass of a standard 7L pot and lid was measured and recorded. The lid was removed from the scale and the pot mass tared. Five kg of 15 °C water was added to the tared pot.
2. The custom instrumentation, including the NDIR analyzers and flow control cart, was initialized for data collection. After a five minute NDIR background sample, the pot, water and lid were moved into the sampling hood on the pot supports of the burner. An Omega k-type thermocouple was inserted through a hole in the lid to the midpoint of the water column.
3. The gas cylinder was opened with the mass flow rate set at 0.052 g/s and ignited at the burner head. The mass of the cylinder and temperature of the water were measured and recorded simultaneously with gas ignition.
4. Keeping a constant flow rate, the NDIR and flow control cart continued to record data as the water's temperature increased. At the ten-minute mark, the gas cylinder was closed and the cylinder mass and water temperature were recorded.
5. The pot of water was immediately removed from the sampling hood for mass measurement and comparison to the pre-test mass of the pot, lid and water.
6. The mass change of the cylinder, or test fuel consumption, was corrected using a carbon mass balance method that utilized the results of the NDIR sampling. The carbon mass balance method can be found in Appendix A.
7. Thermal efficiency was calculated from the results of the carbon mass balance, beginning water mass, change in water mass, change in water temperature and the gas calorific value.



Figure 22 – Left: Measuring 5L of water, Right: Placement of an Omega K-Type thermocouple through the pot lid for the duration of each test

A second set of time controlled ten-minute cold start tests were conducted using a range of mass flow rates that correlate to a range of firepower values from 0.5 kW to 3.0 kW. The three selected flame port geometry designs as well as the original design (four total) were tested over this range to identify how thermal efficiency and emissions change with firepower. Test repetition within the firepower sweep for confidence in the results was not included in this set of tests. The tests followed the same protocol detailed in the above list.

3.2.5.1 Flame Color Analysis

Following the time controlled water boil tests at the low firepower condition, a photo of the flame for each design was taken without the 7L pot. A pixel analysis of the flames was conducted to both quantitatively and qualitatively describe flame structure. The analysis enabled design to design comparison using the number of blue pixels in each photo. The R-Studio® code used for this analysis is located in Appendix A.

A Canon EOS 6D digital SLR camera was used to capture the photos in a dark environment. The exposure time was set to 1/20th of a second, focal length set to 70 mm, ISO speed set to 1600 and the focal-stop set to 7.1.

3.2.6 Off the Shelf Burner Testing

In an effort to understand the performance of off-the-shelf domestic biogas and modified LPG burners, a collection of stoves was amassed. The collection entailed the Puxin dual burner (China), Delher modified LPG stove (Mexico), Rupak single burner (India) and the above mentioned DTW Lotus burner (Cambodia). The stoves were used to gather performance data and to generate trends related to the influence of partially premixed and diffusion flames as well as firepower on stove performance when using biogas as a fuel. This data was not repeated for confidence in the results. Similarly, low confidence data was collected on a series of injector jet and flame port modifications to the Delher LPG stove. A summary of each burner is located in Appendix A and the results of the Delher testing are located in Appendix B.

CHAPTER 4. RESULTS AND DISCUSSION

The following sections detail the outcome of the application of the developed modeling tool toward biogas burner flame port design. The results of the modeling tool enabled a quantitative approach to design selection and comparison before engaging in manufacturing. The experimental results are also presented here and demonstrate the strengths and weaknesses of the tool when applying the theoretical solutions to an experimental environment.

4.1 Modeling Tool

The results of the modeling tool are broken up into two sections: the burner assembly mixing and the flame port combustion simulations. The predictions of the mixing simulation informed the combustion simulation, in which the resulting emissions and temperature values were used to choose three of the nine developed designs.

4.1.1 Burner Assembly Mixing Simulation

The output of the mixing simulation included the mass flow rate of biogas and entrained air and the average velocity of the bulk fuel and air mixture at the flame port. Armed with the mass flow rates of fuel and air, the equivalence ratio for each case was calculated. Although bulk mass flow rates were identical in the ANSYS® and manual calculations, the velocities at the flame port were not. This is likely the result of the restricted geometry of the outer bounds of the mixing model due to limited computational power. The CFD simulation either could not reach mass continuity or there were driving factors that were not easily recognized. Despite this discrepancy, the tool procedure was maintained and the mixing model velocity values were used as inlet conditions for the combustion model.

However, for trends analysis, the manually calculated and continuity conserved velocity values were used to calculate local Reynolds number. Reynolds number was influenced by the velocity, mixture density and hydraulic diameter, all of which change along with geometry.

Table 8 – Equivalence ratio and average port velocity results used to inform the combustion simulation

Design	Description	Phi	Hydraulic Diameter (D_h)	ANSYS® Velocity (cm/s)	Manually Calculated Velocity (cm/s)	Reynolds Number
Original	20 x 5.5 mm D shape	2.95	0.529	28.3	27.7	129
1a	48 x 4 mm circular	2.95	0.406	23.8	22.2	79
1b	32 x 5 mm circular	3.02	0.490	28.0	22.5	97
1c	22 x 6 mm circular	2.90	0.596	26.8	22.8	120
2a	19, 8 x 4 mm rect.	2.93	0.533	25.9	24.2	113
2b	38, 8 x 2 mm rect.	2.98	0.322	22.6	22.6	64
2c	58, 8 x 1.3 mm rect.	3.04	0.228	22.1	22.2	44
3a	14 x 4 mm circular 14, 8 x 4 mm rect.	2.76	0.495	22.7	23.2	101
3b	17 x 4 mm circular 17, 8 x 3 mm rect.	2.72	0.423	21.6	23.6	88
3c	27 x 3 mm circular 27, 8 x 2 mm rect.	2.79	0.314	22.8	23.1	64

4.1.1.1 Visual Representations

The mixing model also tracked the movement of species through the 3-D rendering, including nitrogen and oxygen in air and methane and carbon dioxide in biogas. By calculating the nitrogen mass fraction at each point of the 3-D rendering, the entrainment effect was visualized (Figure 23). This visual provided confirmation that the air and fuel was homogeneous at the flame port.

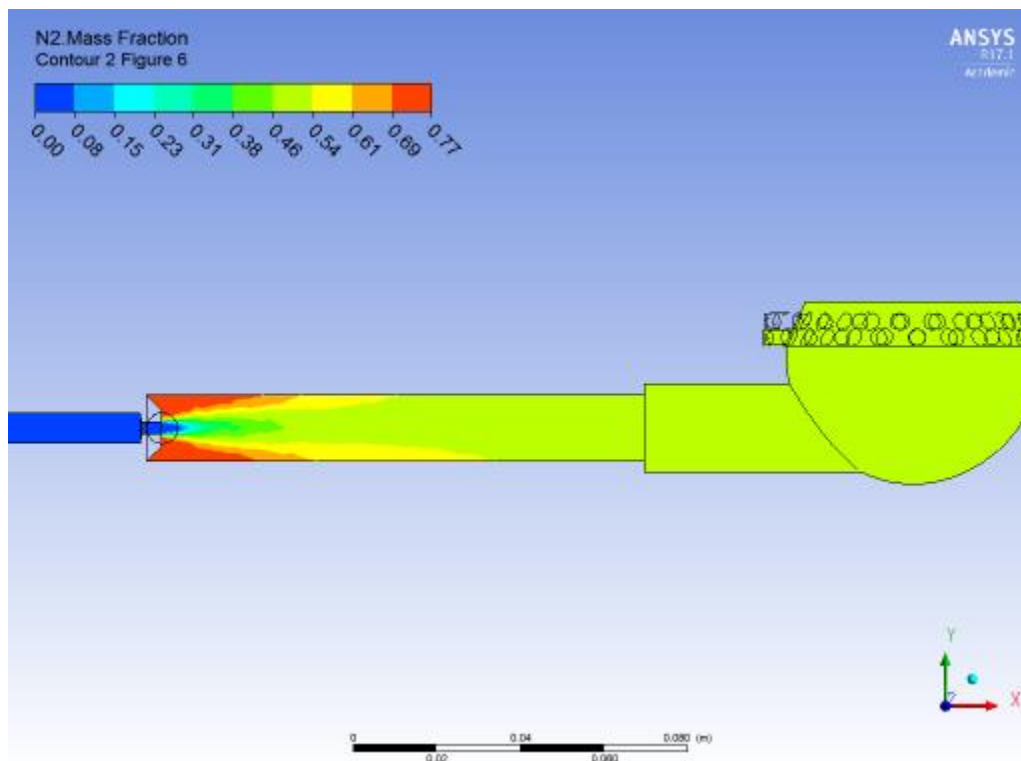


Figure 23 – A visualization of the entrainment effect of air and extent of homogeneity in the mixture for design 1a

By plotting the velocity vectors within the 3-D rendering, an even deeper understanding of the entrainment effect was realized. As gas enters the injector orifice in the burner, cross sectional area reduces drastically, leading to an increase in velocity per the continuity equation. Once the gas exits the injector orifice, the cross-sectional area widens back out, reducing gas velocity. This change in velocity creates a low-pressure zone and gradient between the ambient surroundings and the inside of the burner, pulling air into the burner throat.

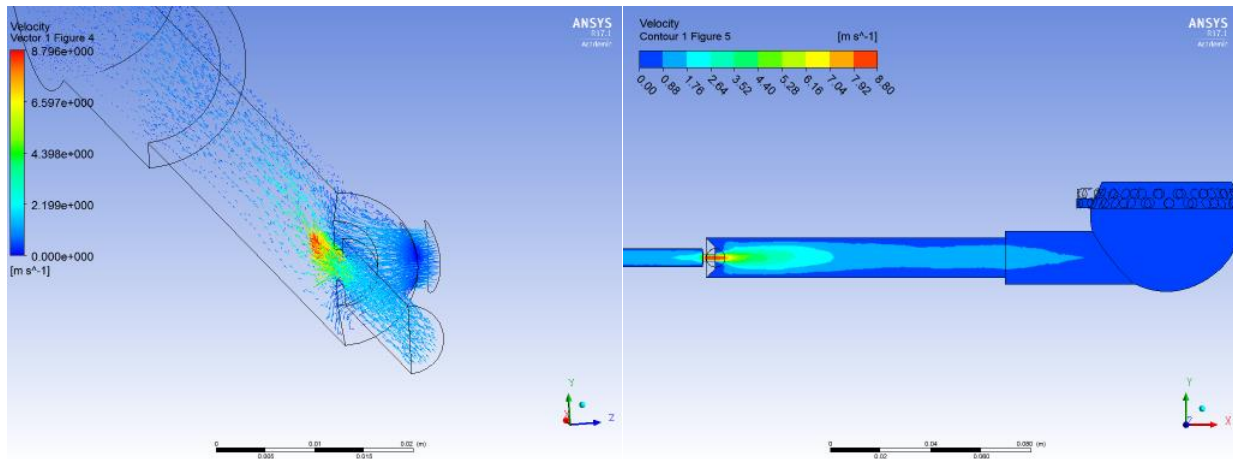


Figure 24 – Velocity contours and vectors illustrating the entrainment of ambient air into the burner throat for a partially premixed flame for design 1a

4.1.2 Flame Port Combustion Simulation

The output of the flame port combustion simulations included the mass flow rate of emissions species and reaction temperatures within the external combustion volume. The zone temperature was calculated as an average of the external volume and the maximum temperature represents the hottest part of a flame near or at the stoichiometric mixture front. Using the mass flow rate of CO and CO₂, the modified combustion efficiency was calculated for each case.

Table 9 – Results from the flame port combustion simulation

Design	Exhaust-CH ₄ (kg/s)	Exhaust-CO ₂ (kg/s)	Exhaust-CO (kg/s)	Combustion Efficiency	Zone Temperature (K)	Max Temperature (K)
Original	6.32 E-07	1.33 E-05	5.1 E-07	96.3%	486	1770
1a	4.34 E-08	1.09 E-05	1.4 E-07	98.7%	627	1876
1b	1.11 E-07	2.42 E-05	4.48 E-07	98.2%	639	1835
1c	1.49 E-07	1.80 E-05	2.88 E-07	98.4%	585	1803
2a	1.05 E-07	1.81 E-05	2.38 E-07	98.7%	588	1856
2b	3.48 E-07	1.44 E-05	1.19 E-06	92.4%	583	1910
2c	5.62 E-07	1.62 E-05	1.46 E-06	91.8%	561	1926
3a	2.27 E-07	1.48 E-05	5.01 E-07	96.7%	618	1823
3b	1.1 E-07	1.53 E-05	3.37 E-07	97.9%	684	1893
3c	2.75 E-07	1.55 E-05	7.21 E-07	95.6%	659	1910

4.1.2.1 Emissions

The modeling tool predicted lower carbon monoxide emissions than the original for six of the nine designs and lower unburned methane for all of the nine designs (Figure 25). Modified combustion efficiency was calculated for each design and three of the nine designs performed at lower efficiency than the original (Figure 25). However, previous studies by Turanyi et al. and Kong and Reitz have shown that results from chemical kinetics simulations can be highly variable and uncertain, providing more encouragement to perform experimental tests [45], [46].

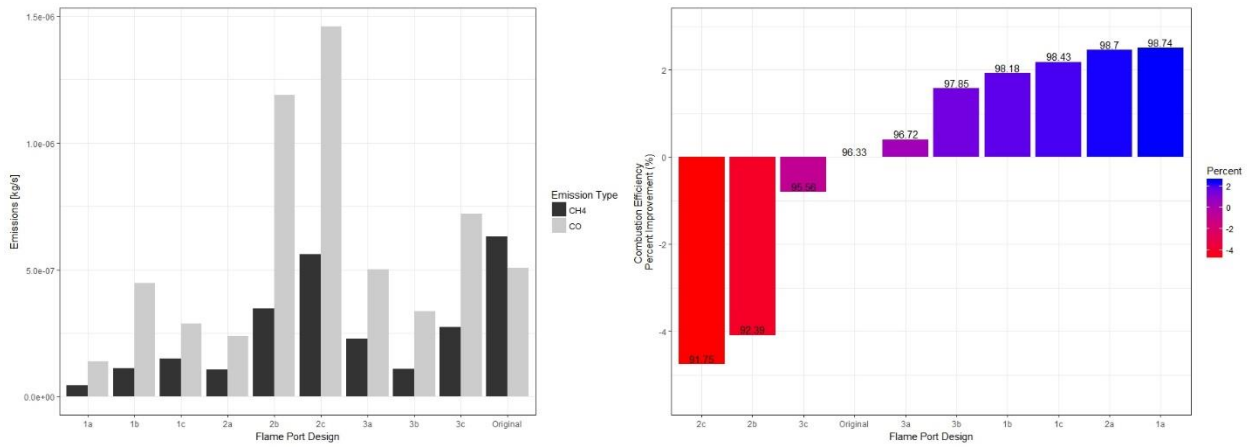


Figure 25 – Top: CO and CH₄ emissions comparison for all nine designs against the original, Bottom: Changes in combustion efficiency due to port geometry compared to the original design

4.1.2.2 Temperatures

The modeling tool predicted improved zone and maximum temperatures for each of the 9 designs compared to the original (Figure 26). Zone temperatures improved between 15 to 40 percent and maximum temperatures improved between two and nine percent. Since no heat transfer modeling for a simulated water boil test was conducted, these temperature values were used as a proxy for thermal efficiency. When considering thermal efficiency, a higher zone temperature is likely to have a larger influence than a higher maximum temperature. Maximum temperatures may only occur in small localized regions and provide marginal improvements to the three modes of heat transfer. See Section 4.1.6 to see how the rank of maximum temperatures align

with the rank of zone temperatures for the same design. Case in point, design 2c has the highest ranked maximum temperature, but is ranked second to last in zone temperature.

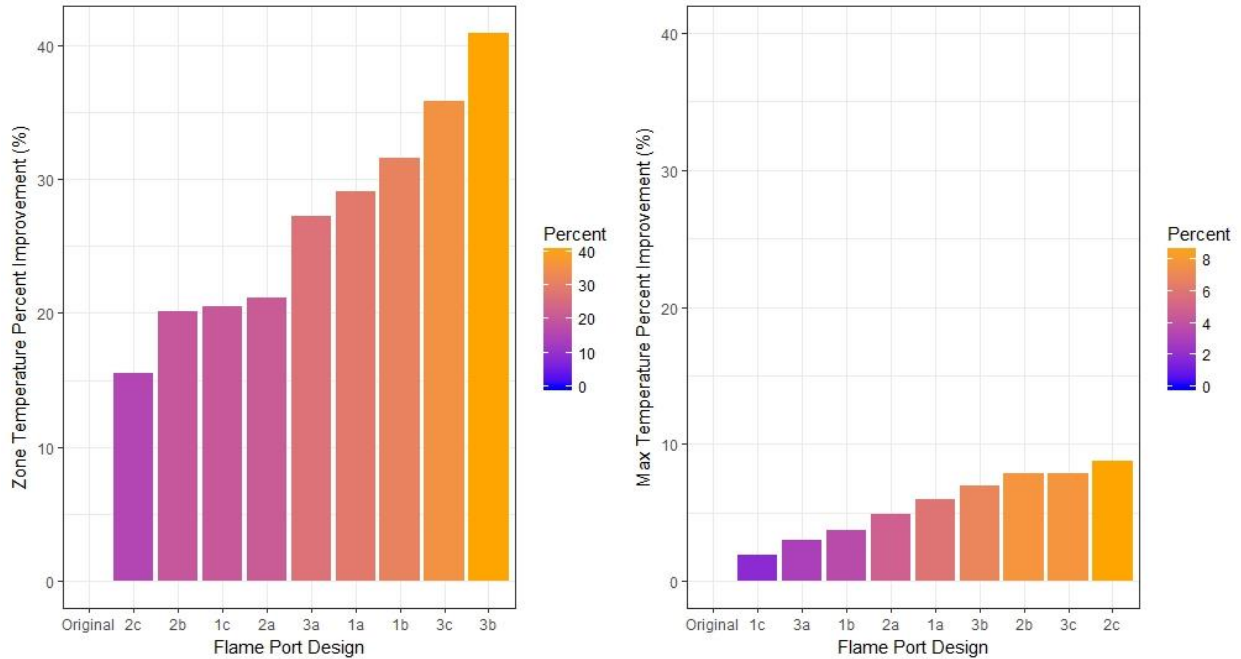


Figure 26 – The influence of port geometry design changes on zone and maximum temperatures

4.1.2.3 Visual Representations

The simulation produced visuals that identified the high temperature regions of the flame as well as the extent of increased temperature throughout the external volume. The maximum temperature results passed one level of validation by remaining below the adiabatic flame temperature of 2100 K as calculated by Chemkin® and shown in Appendix A. This means that as expected, the temperature at the stoichiometric mixture front in the simulation could not reach adiabatic levels due to various losses. The temperature values in the simulation were used for design selection only. Flame temperature data was not collected in an experimental setting for comparison.

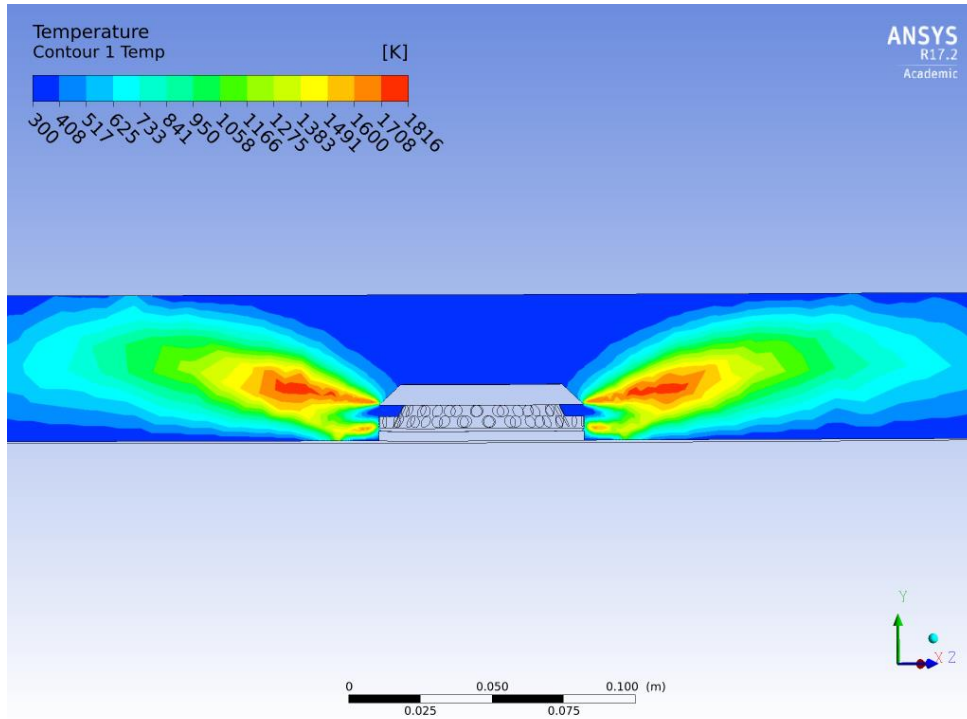


Figure 27 – Temperature contour due to combustion within design 1a

The simulation also produced telling visuals de scribing velocity flow profiles in circular ports. As expected, surface friction at the port walls reduced velocity and created a parabolic profile with the highest flow velocity in the middle of the port. Rectangular ports had a visibly more homogenous profile due a greater aspect ratio.

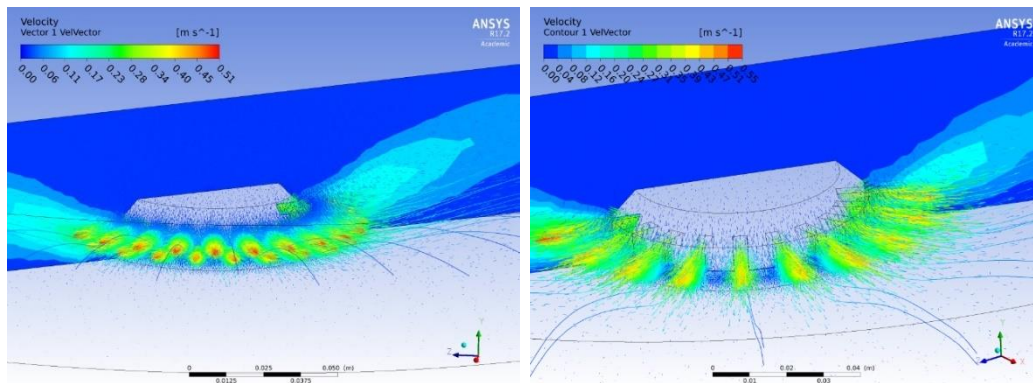


Figure 28 – Velocity contours for design 1a showing a parabolic condition within circular ports

4.1.3 Port Geometry

Port geometry was the main factor in this study. The results from the mixing and combustion simulation suggested several relationships between port geometry and predictor variables.

Establishing the relationships began with understanding how port geometry could be represented. Using geometric ratios summarized by H.R.N. Jones from previous burner studies, port geometry was related to hydraulic diameter. These ratios were depth to diameter for circular ports (designs 1a, 1b and 1c), length to width for rectangular ports (designs 2a, 2b and 2c) and a weighted average between the two factors for a combination of circular and rectangular ports (designs 3a, 3b and 3c). For all three of the design cases, as the ratio factor for port shape increased, hydraulic diameter decreased.

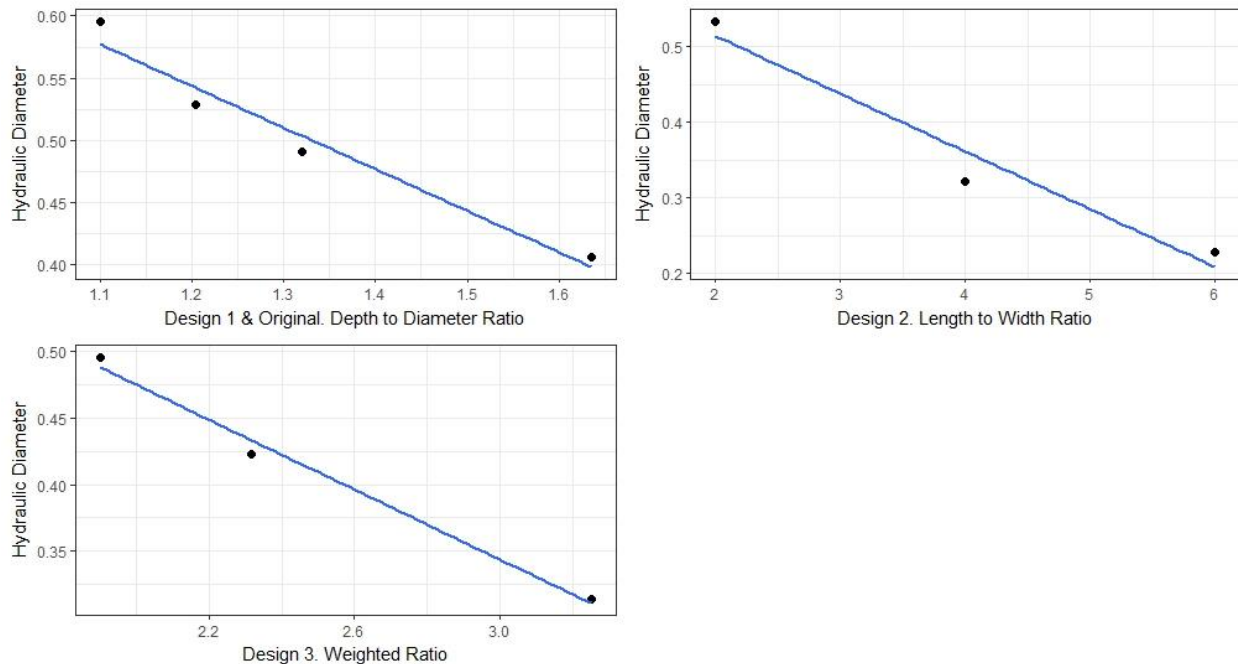


Figure 29 – Port shape ratio factor as a function of hydraulic diameter (D_h)

As described in Section 1.5.1, mixture density and velocity are also influenced by changes in port geometry. Since fuel flow rate was constant in the model, mixture density was dependent

on the bulk flow rate and corresponding equivalence ratio, which varied for each design within the modeling tool. This was a result of a change in pressure drop with geometry, influencing the pressure gradient immediately following the injector orifice. A similar relationship was found in an LPG burner study by Wong et al. in which variations in pressure drop and consequently equivalence ratio were found due to changes in system configuration [47].

Figure 30 shows that as expected, an increase in bulk mass flow rate corresponds with a decrease in equivalence ratio and increase in mixture density ($R^2 = 0.99$). This means that when more air was entrained into the burner, the ratio of stoichiometric air to fuel fraction to actual air to fuel fraction goes down. In this case, the density of air is higher than that of a 60 mol% methane biogas, leading to an increase in mixture density with bulk mass flow when fuel flow is constant.

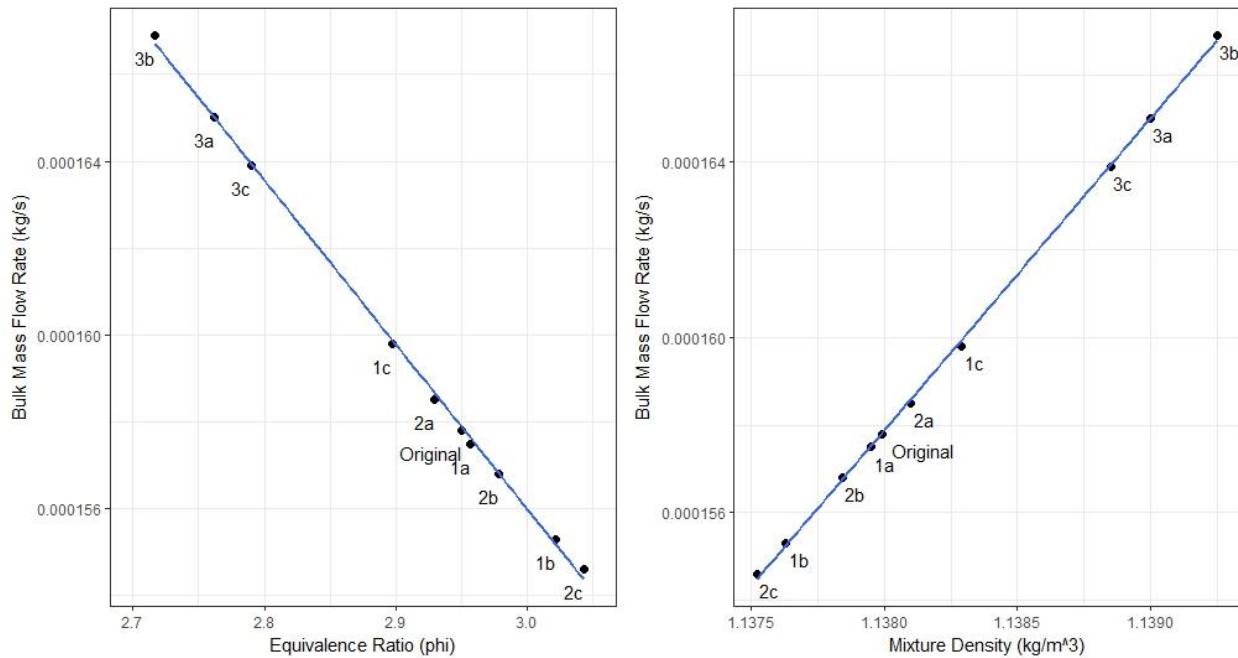


Figure 30 – Display proving the direct and linear relationship between bulk mass flow rate and mixture density with equivalence ratio

Per several studies that have investigated the influence of equivalence ratio, the ideal combustion case for partially premixed burners is the entrainment of 60 % of the stoichiometric

air requirement or an equivalence ratio of 1.66 [14]. This is a fuel rich condition in which the remaining quantity of required air diffuses into the flame front. Each of the ten designs simulated were more fuel rich than the optimized phi value of 1.66. Within the designs, five of the nine developed in this study led to an increase in aspirated air, or a phi closer to 1.66 as compared to the original. Theoretically the amount of increase of aspirated air in these five designs toward the phi of 1.66 range would increase flame temperatures and combustion efficiency. A design with a phi of less than 1.66 may lead to an increased chance of flame lift off due to the increased velocity of the bulk flow outcompeting the movement of the stoichiometric mixture front closer to the port surface. When considering heat transfer and thermal efficiency, there is a point where an increase in thermal mass due to the aspiration of greater amounts of air outcompetes the increase in flame temperatures due to more complete combustion. This point varies depending on design but certainly occurs once phi drops below 1 and the bulk flow enters a fuel lean condition.

Additionally, since this study did not change total port area, the continuity equation demands that as bulk mass flow changes, density and/or velocity must change. By combining the three factors influenced by geometry (hydraulic diameter, velocity and mixture density), a multiple linear regression analysis was conducted using the Matlab® rstoool (Figure 31) to understand their relationship to the four model predictors used for design comparison (Section 2.3.4). This analysis method has been used in various design of experiment studies and was also applied to the experimental results [48]. For the model results, the following null hypotheses were tested (n=10).

$$H_0: \frac{\partial \text{zone temperature}}{\partial D_h, \partial v, \partial \rho} = 0, \quad H_0: \frac{\partial \text{maximum temperature}}{\partial D_h, \partial v, \partial \rho} = 0, \quad H_0: \frac{\partial \text{total hydrocarbons}}{\partial D_h, \partial v, \partial \rho} = 0, \\ \text{and } H_0: \frac{\partial \text{combustion efficiency}}{\partial D_h, \partial v, \partial \rho} = 0$$

The null hypothesis could only be rejected for five out of the 12 cases (as indicated by the asterisk in Table 10). Notably, velocity and mixture density have a significant relationship to zone

temperature, hydraulic diameter with maximum temperature and velocity and hydraulic diameter with the amount of total hydrocarbons emitted. Since n is small for this study, a greater number of model iterations may provide stronger evidence of these relationships.

Table 10 – Relationship strength indicators for the influence of factors upon the model predictors

Factor	P-Value			
	Zone T	Max T	Total Hydrocarbons	Combustion Efficiency
Hydraulic Diameter	0.9714	0.00259*	0.0439*	0.0146*
Velocity	0.0295*	0.10531	0.0175*	0.3849
Mixture Density	0.0252*	0.32359	0.2198	0.4241

To maximize zone temperature, the relationships show that mixture density should be increased and the velocity decreased. This means that within the data provided by the model, increasing the amount of entrained air and approaching the ideal phi (1.66), zone temperature can be increased. To minimize total unburned hydrocarbons, velocity should be minimized and hydraulic diameter maximized. The most significant relationship was to maximize maximum temperature; hydraulic diameter should also be maximized. The magnitude of the slope of the responses show the amount of influence that each of the design factors has on that predictor. Other relationships can be explored by viewing the linear regression trendline in each relationship box in the prediction profiler below.

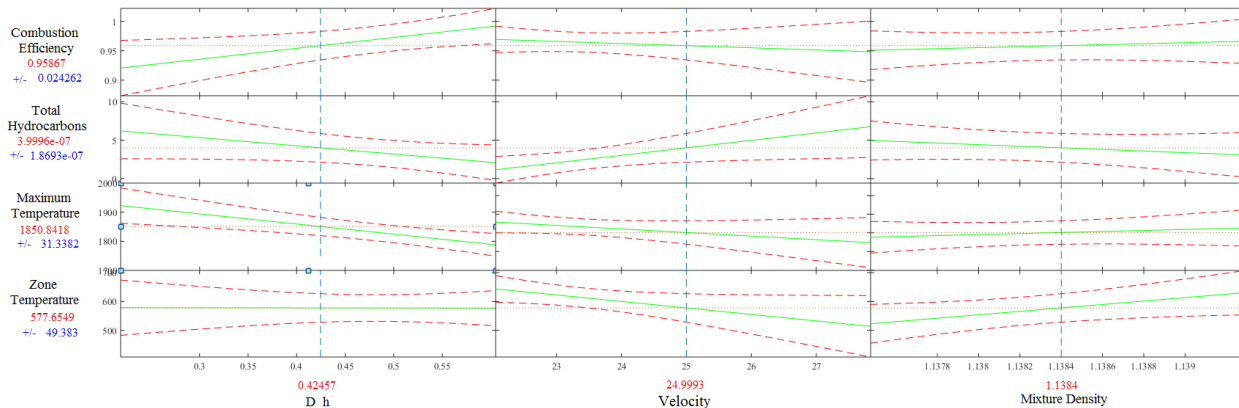


Figure 31 – Matlab® rstool prediction profiler to establish a design response surface for desired predictor values

An alternative approach to understand factor and predictor relationships, that was not used in this study, would be to leverage Reynolds number's dependence on hydraulic diameter, velocity and mixture density (Figure 32) [49].

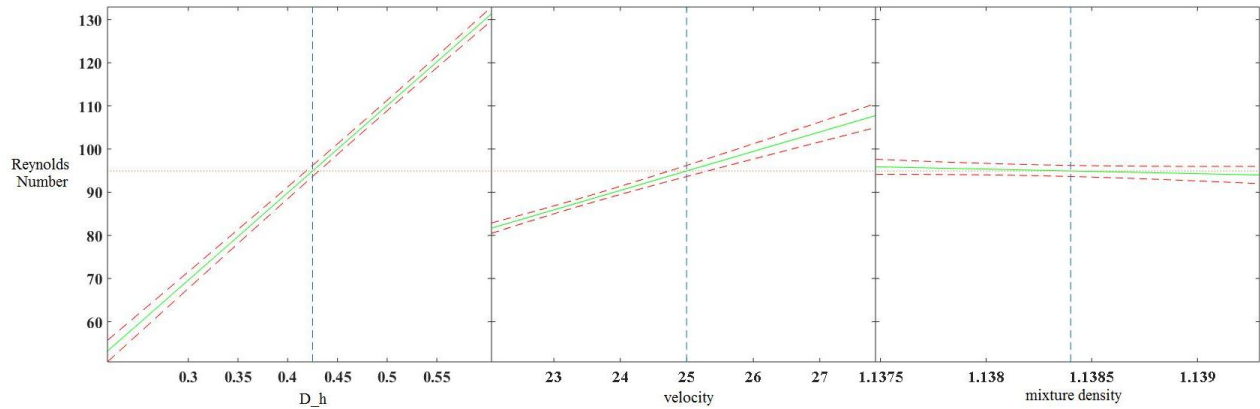


Figure 32 – Results of a multiple linear regression: $lm(\text{Reynolds} \sim D_h + \text{velocity} + \rho_{\text{mixture}})$

However, the dependence of Reynolds number on these three factors causes multicollinearity. This makes linear modeling via hypothesis testing difficult and misleading, often compounding error embedded in the connections between the three factors (D_h , v and ρ_{mixture}) and the performance predictors [50]. Lasso or ridge non-linear regression modeling may result in the creation of more meaningful relationships between Reynolds number and the performance predictors. Previous LPG studies by Wong et al. have utilized Reynolds number to predict performance trends [49].

4.1.4 Port Spacing

Previous studies summarized by H.R.N. Jones and Wong indicated that the distance from port to port plays a role in flame stability and combustion [14], [51]. However, the results from this study did not suggest any significant relationships between emissions and temperature predictors with port spacing (Figure 33, $H_0 : \frac{\partial \text{performance predictors}}{\partial \text{port spacing}} = 0$, $n = 10$, $p > 0.1$ for all tests). This may be a function of the low firepower setting of the model simulation. Port spacing

becomes more important with increasing firepower, as higher port velocities at higher firepower lead to unstable flames. Further confirmation of the role of port spacing by conducting simulations at higher firepower is needed to make exploratory recommendations.

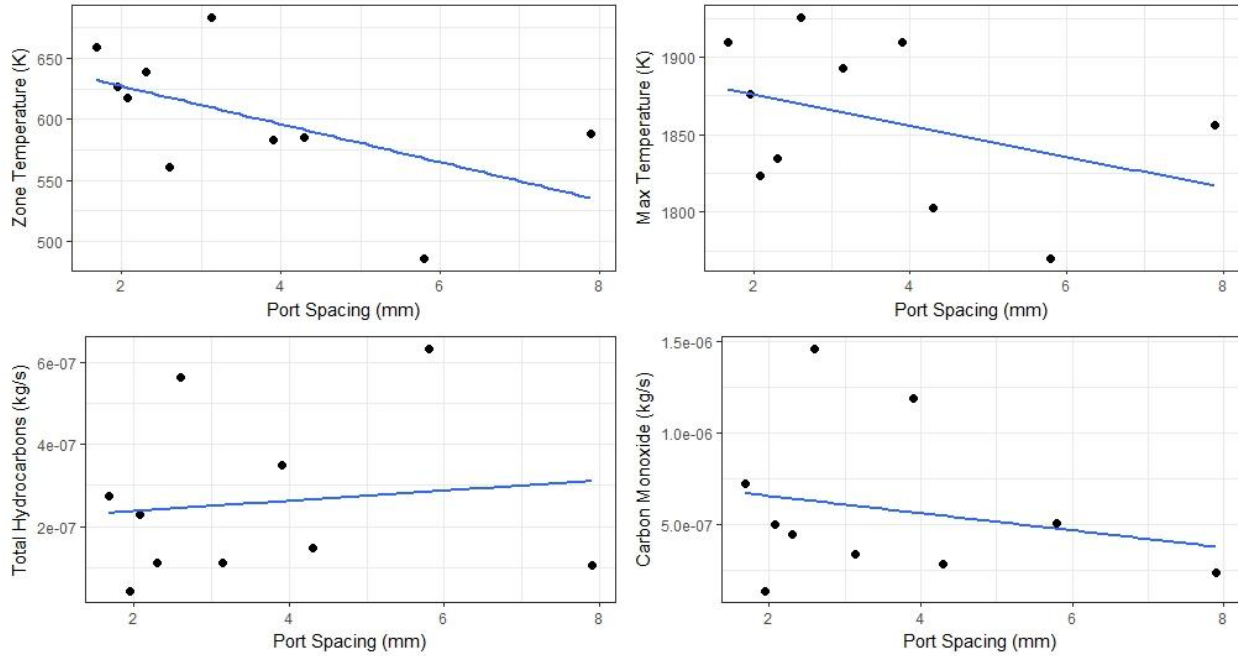


Figure 33 – A display of wide variations and little to no correlation between port spacing and performance predictors

4.1.5 Port Design Rank

The performance predictors, zone temperature, maximum temperature, unburned methane emissions and combustion efficiency, were equally weighted and ranked per design to compare the nine developed designs against the original. The top three ranked designs, 1a, 3b and 2a were selected for manufacturing and testing in a physical setting.

Table 11 – Results of the equal weighted ranking procedure to determine the top three designs

Design	Zone Temperature [K]	Max Temperature [K]	Methane Emissions [kg/s]	Combustion Efficiency	Total	Rank
1a	4	5	1	1	11	1
3b	1	4	3	5	13	2
2a	6	6	2	2	16	3
1b	3	7	4	4	18	4
3c	2	2	7	8	19	5
1c	7	9	5	3	24	6
3a	5	8	6	6	25	7
2b	8	2	8	9	27	8
2c	9	1	9	10	29	9
Original	10	10	10	7	37	10

The highest ranked design, 1a, mirrors the results reached by Jadhav et al. in their CFD study that the optimal flame port diameter for biogas burners is four millimeters [22]. Design 1a ranked first in both emissions categories, suggesting that the parabolic flow profile as explained in Section 4.1.2.3 specific to four-millimeter diameter ports positively contributes to fuel combustion and flame stability.

Amid the ranking process, a few trends emerged. As diameter and length to width ratio for circular and rectangular ports increase, rank decreases. For rectangular ports, two out of the three designs ranked in the bottom third. The rank of methane emissions loosely follows the order of the total rank, while the rest of the predictors are fairly scattered.

4.2 Experiment

The results of the experiment included the following; comparisons between premixed and diffusion flames, time and temperature controlled water boil tests for the chosen flame port designs (1a, 2a and 3b) compared to the original and a series of water boil tests of off the shelf burners.

4.2.1 Off the Shelf Burner Testing

4.2.1.1 Influence of Flame Type

Using the lotus burner at an upper firepower setting (~ 4 kW), Figure 34 shows qualitative differences between a partially premixed and diffusion flame. The partially premixed flame was shorter and more robust. The stoichiometric mixture front was pulled closer to the flame port due to a lesser amount of diffused air required to achieve ϕ of 1. The diffusion flame was stretched due to all the required air to achieve a ϕ of 1 being sourced from the space surrounding the flame. Thus, there was a greater chance of incomplete combustion, allowing for a greater amount of unburned hydrocarbons and carbon monoxide to enter the emissions stream.



Figure 34 – Left: Partially premixed flame, Right: Diffusion flame

Temperature controlled water boil tests were conducted at an upper firepower setting (~ 4 kW) across five burners; Lotus, Puxin, Rupak, Delher Case 2 and Delher Case 3. A test was

conducted for each burner with (partial premixing) and without (diffusion) the aspiration of air. For each burner, the carbon monoxide emissions (g/MJ_d) were drastically reduced by incorporating air entrainment, effectively improving combustion efficiency. For upper firepower, total grams of carbon monoxide indicates the level of acute risk during a cooking event.

In all but one case at the upper firepower setting, thermal efficiency decreased by entraining air even though combustion efficiency increased. This was likely due to the increased thermal mass of a premixed fuel flow outcompeting the benefit of a higher combustion efficiency. This could also be due to increased radiative energy from the luminous combustion of soot particles [13]. Additionally, at an upper firepower setting, the Puxin and Rupak stoves landed in Tier 3 for efficiency, while the majority of the Lotus and Delher stoves landed in Tier 2. All of the burner iterations were at the highest tier (Tier 4) for emissions, as expected. Compared to biomass, gaseous fuel emissions in burners often emit lower concentrations of carbon monoxide [52].

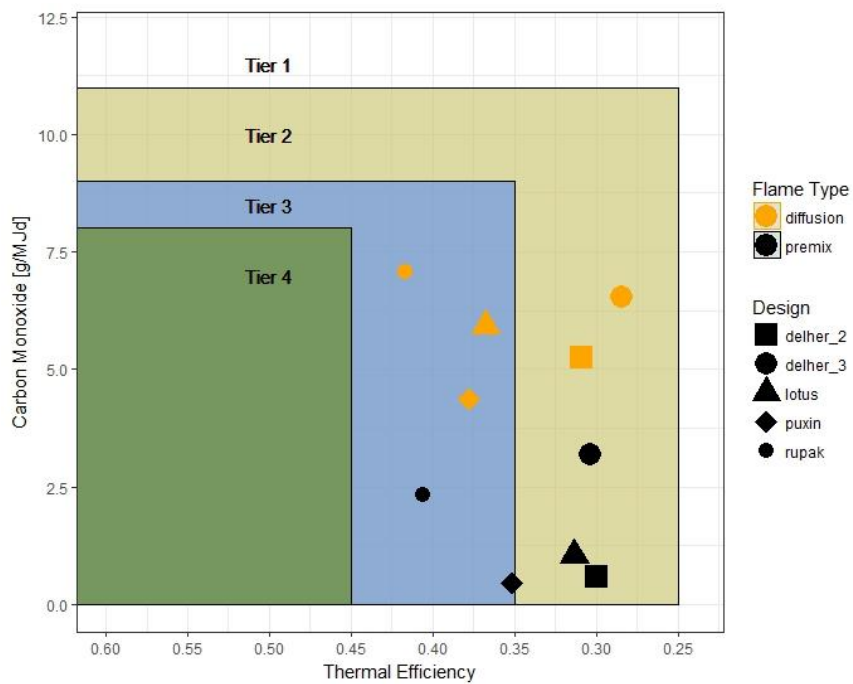


Figure 35 – Upper firepower flame type comparison water boil tests using the IWA tier structure

Since this study focused on the Lotus burner at a low firepower condition, a partial premix test and a diffusion test for the Lotus were conducted at a firepower setting of roughly one kilowatt. By entraining air, both the thermal efficiency and level of carbon monoxide emissions improved. At lower firepower, these results suggest that the improvement in combustion efficiency outweighs the increase in thermal mass (for partially premixed compared to diffusion), leading to an improvement from Tier 2 to 3. Hence, all further experimental tests at lower firepower were conducted in a partially premixed fashion.

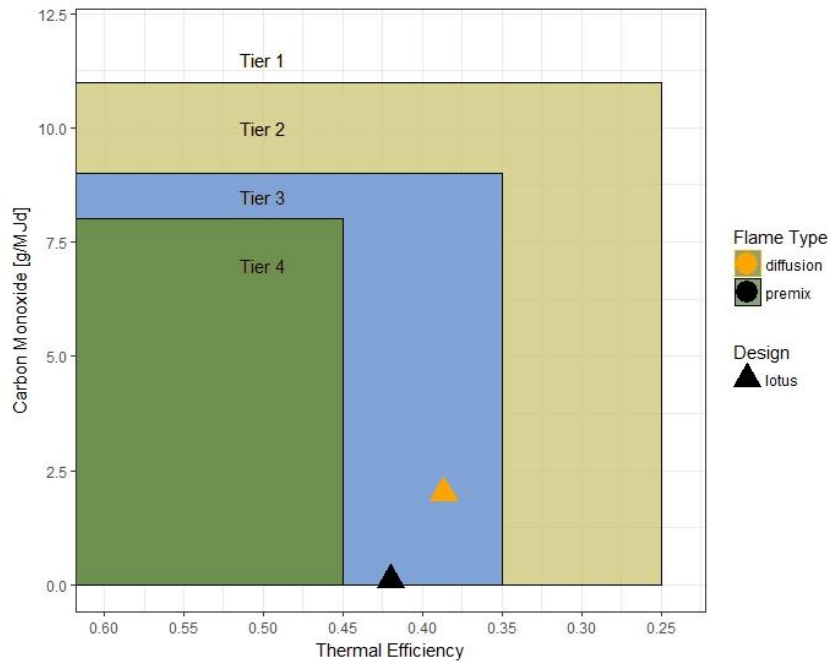


Figure 36 – Lower firepower flame type comparison WBT for the Lotus burner

Note that all tests in this section (4.2.1) were exploratory. The findings were intended to explore trends in flame type and did not validate or verify any of the conclusions made here.

4.2.1.2 Influence of Firepower

A series of temperature controlled water boil tests were conducted to evaluate the influence of firepower on emissions and heat transfer. The tests included the Lotus and Puxin burner at a lower (~ 1 kW) and upper (~ 4.5 kW) firepower setting with a partially premixed flame. Within

the cases tested, increasing firepower led to a decrease in thermal efficiency and increase in carbon monoxide. Combustion efficiency drops with an increase in firepower because bulk velocities increase, leading to an increase in the incomplete conversion of methane to carbon dioxide.

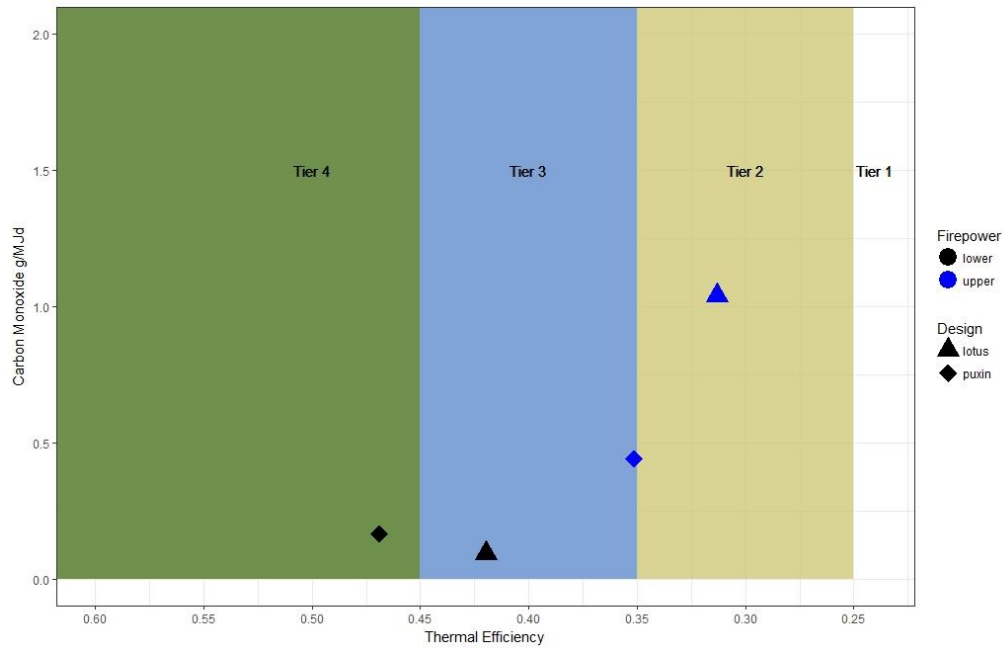


Figure 37 – An exploration of the influence of firepower on emissions and heat transfer

4.2.1.3 Particulate Matter Emissions

Particulate matter emissions were collected at low (~ 1 kW) and upper firepower (~ 4.5 kW) settings among a variety of nine temperature controlled water boil tests using the Lotus burner. Both partially premixed and diffusion flames were tested. Out of the nine tests, eight met the limit of detection and two met the level of quantification. This means that the study could only be certain of the quantity of particulate matter collected for two of the tests, suggesting that PM emitted from the Lotus burner was significantly low.

Since only two tests could be analyzed, no real trends or internal relationships regarding PM could be established for the Lotus burner. To understand the magnitude of PM emitted, the two PM values from this study were compared against PM values emitted from woody biomass

cookstoves. A study by Grieshop et al. showed a range of PM (g/kg of fuel) from 2.1 – 8.5 for traditional and improved biomass stoves and 0.5 – 1.1 for biomass gasifier stoves [39]. The two quantifiable PM values recorded in this study were 0.1 and 0.045 g/kg of fuel, roughly 5-85 times lower than biomass stoves.

Per the above confirmation regarding the suggestion by Grieshop et al. that PM is negligible for gaseous burners, PM measurements were not recorded for the remainder of the study. Detailed results from the PM portion of this study can be found in Appendix B.

4.2.2 Time Controlled Protocol

Using the time controlled protocol (10-minute duration water boil test starting at 15°C), two series of tests were conducted with the Lotus burner only; tool validation at low firepower and an exploratory firepower sweep. These tests were conducted using the three selected designs from the tool as well as the original design.

4.2.2.1 Low Firepower Condition

This series of experimental tests was intended to corroborate the findings of the modeling tool. The tool suggested designs 1a, 3b and 2a were the top performers, and had an overall rank higher than the remaining seven designs, including the original. The tests were repeated between three and four times for each of the four designs (1a, 3b, 2a and the original) at a fuel flow rate that was +/- 10% of the constant rate set in the modeling tool (0.052 g/s).

Thermal Efficiency

By measuring water temperature and conducting a carbon balance of the emissions stream to determine the mass of fuel consumed, thermal efficiency for each test was calculated. Each of the three chosen designs resulted in higher thermal efficiencies compared to the original, with the order of improvement following the prediction of the tool. In other words, the predicted rank of

the designs in the tool matched the rank of designs when considering thermal efficiency only, suggesting that the tool is a justifiable way to predict thermal efficiency.

Table 12 – Thermal efficiency summary

1.1 kW Firepower +/- 10%		
Design	Mean	% Gain
1a	56.8 %	7.17 %
3b	55.1 %	3.96 %
2a	53.5 %	0.94 %
Original	53.0 %	0.00 %

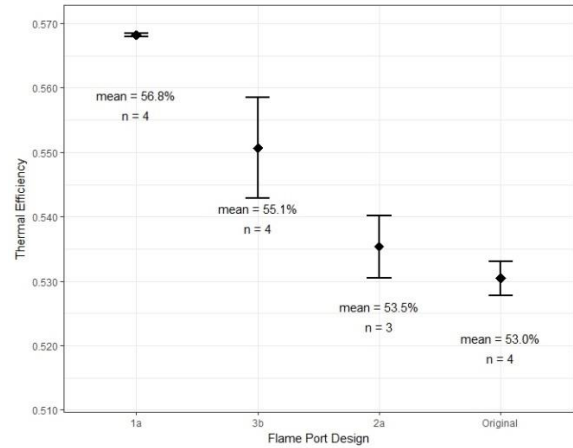


Figure 38 – Thermal efficiency results from the time controlled, low firepower condition

Of similar significance as the trend in thermal efficiency was the variance of efficiency between tests for each design. Design 1a, compared to the remaining 3 designs tested, had a noticeably tighter confidence interval. This means that the results of each test were comparatively precise. The precision of design 1a suggests that the arrangement of four mm diameter circular ports results in a stable and consistent flame.

Photo Analysis

The photos taken of each design at the low firepower setting were analyzed to depict the percentage of blue pixels for inter-design comparison. This study attempted to create a relationship between the generation of blue color and the tested thermal efficiency. Although a direct linear relationship was not found, an overall trend was established. Designs 1a and 3b had a greater percentage of blue pixels and higher thermal efficiencies than designs 2a and the original. The increasing trend of blue pixels among designs did however match the increasing trend of zone and maximum temperature improvement in the modeling tool. See the below emissions section for a qualitative analysis of the photos.

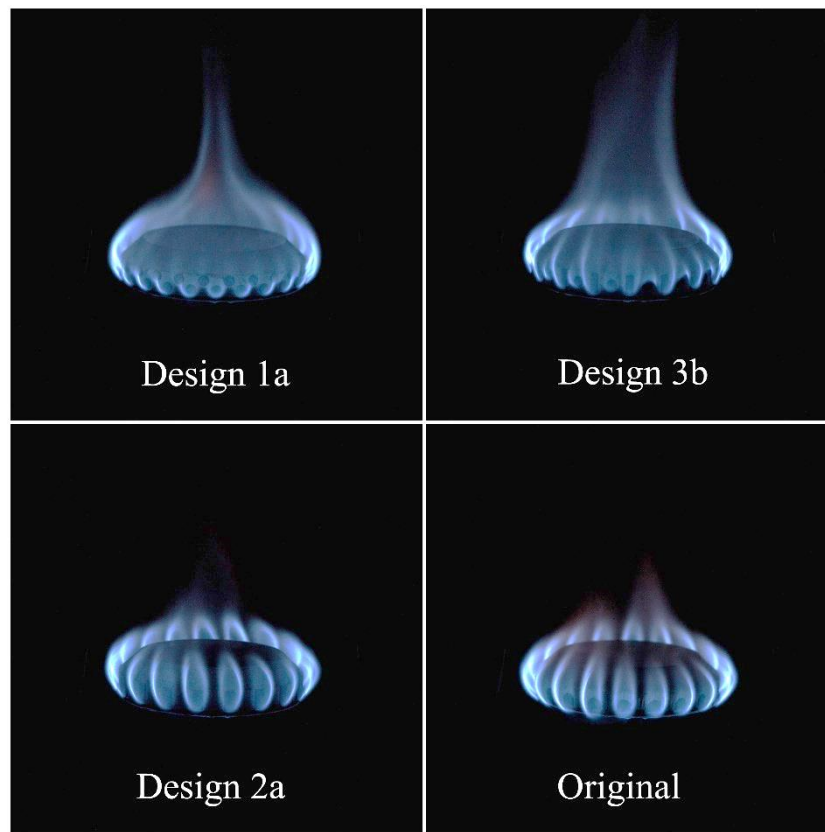


Figure 39 – Identical flame photos of each design providing for qualitative and quantitative analysis

Table 13 – Summary of predictor variables describing each of the experimentally tested designs

	1a	3b	2a	Original
Thermal Efficiency	56.8%	55.1%	53.5%	53.0%
Model Equivalence Ratio	2.96	2.72	2.93	2.95
Number of Blue Pixels	2.52 E06	2.68 E06	2.36 E06	2.33 E06
Total Number of Pixels	2.99 E07	2.99 E07	2.99 E07	2.99 E07
Percentage of Total Pixels that are Blue	8.39 %	8.94 %	7.87 %	7.76 %

Emissions

The emissions collected for each test included carbon monoxide, carbon dioxide and total unburned hydrocarbons. After data analysis was conducted, a conflicting trend emerged; the designs with higher thermal efficiency resulted in higher carbon monoxide and total unburned hydrocarbon emissions. Higher carbon monoxide emissions thus led to lower combustion efficiencies, which ranged from 98.5 to 99.5%. In comparison, a study of biomass cookstoves resulted in combustion efficiencies of 84 – 94 % [53]. This suggests a superior nature of fuel to heat conversion and CO emissions of biogas burners to biomass cookstoves.

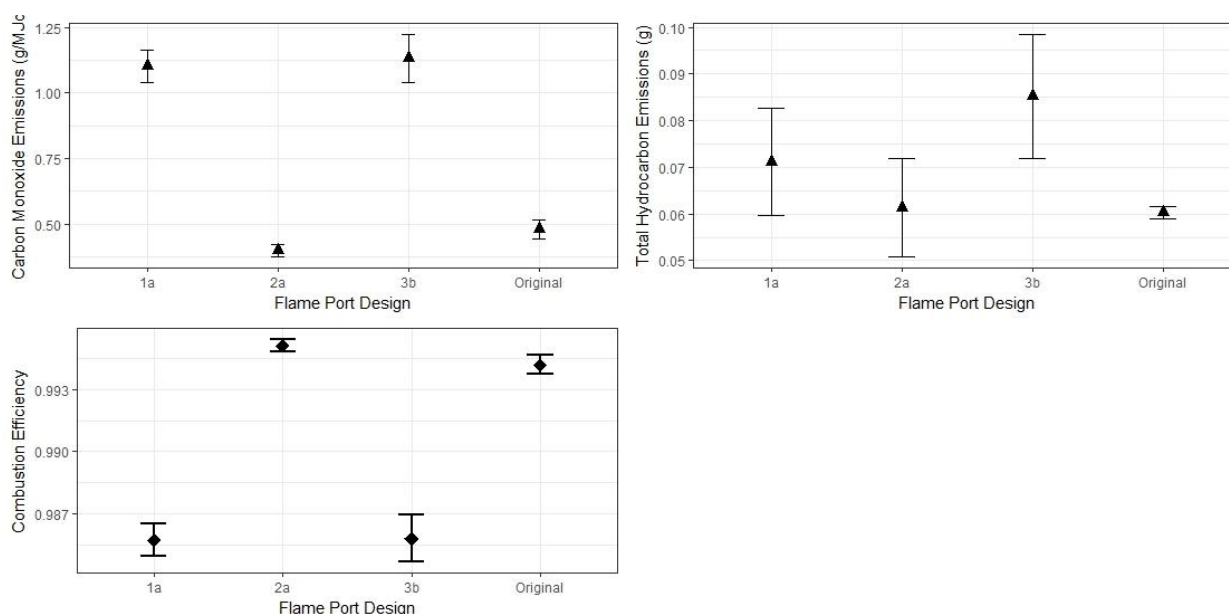


Figure 40 – Experimental emissions results for each flame port design

The conflicting trend may be described by the results of the photo analysis (Figure 39). The top two photos, designs 1a and 3b, had distinct flame stretch. In comparison, designs 2a and the original had wider and shorter flames, closer to the port. These qualitative differences suggest that designs 2a and the original entrained greater amounts of air than 1a and 3b, allowing for the stoichiometric mixture front to be pulled closer to the port surface. Therefore, a more stable flame was created and lower amounts of carbon monoxide and total hydrocarbons were emitted. Regarding heat transfer, the aspiration of more air likely had unbalanced consequences. By increasing bulk flow, a greater mass had to be heated and a comparatively lower amount could be transferred to the pot. Hence, for designs 2a and the original, the increase in combustion efficiency did not seem to outweigh the consequence of an increased thermal mass.

In the experimental portion of the study, the bulk flow rate was not measured or controlled, so the above explanation is exploratory. Table 13 lists the equivalence ratios recorded in the model, which do not provide evidence to support the above argument, but may expose a difference between the modeling tool and experimental testing. To validate the thermal mass explanation, further testing is required where bulk flow rate is controlled.

A second explanation of the conflicting trend may be related to the flame of each respective design's ability to transfer heat to the pot. A stretched flame may indicate higher port velocities, which could compress the boundary layer around the pot and increase the convective heat transfer coefficient. A stretched flame may also increase conductive heat transfer by effectively 'licking' the bottom of the pot. In this study, port velocities were not measured and could not be calculated without knowing bulk flow.

Comparison to the Modeling Tool

Data collected in the experiments allowed for the creation of relationships to the modeling tool. The same emission categories predicted in the tool were tested experimentally, but flame temperature values were not collected for comparison to the model. Instead, thermal efficiency was used as a proxy.

As expected, the emissions predicted in the tool were not representative of actual emissions (see Section 4.1.2.1). Modeling combustion products is difficult and complex and was limited in the model by the extents of the external volume. The consistent error and under-measurement of carbon dioxide in the model suggests that the external volume was not large enough to capture the entirety of carbon dioxide emitted.

Table 14 – Compared percent error of model and experimental emissions results

Design	Percent Error of Model Emissions Predictions		
	Carbon Monoxide	Total Hydrocarbons	Carbon Dioxide
Original	89.9 %	532 %	82.8 %
1a	78.5 %	63.5 %	85.8 %
2a	5.78 %	3.3 %	76.7 %
3b	49.3 %	22.5 %	80.5 %

In contrast to the varying and erroneous carbon monoxide and total hydrocarbon predictions for designs 1a, 3b and the original, the model seemed to predict these experimental emissions for design 2a quite well. More testing and simulation combinations need to be explored to generate an explanation for this finding, but this study suggests that the tool may be better suited to predict emissions from a design of only rectangular ports.

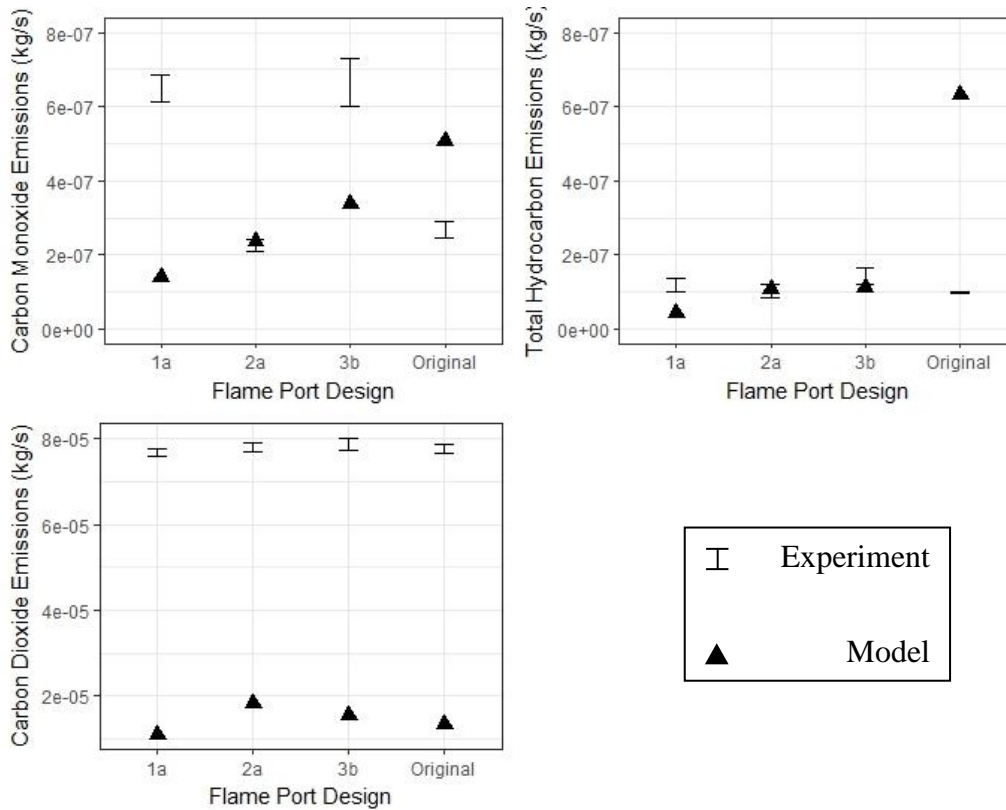


Figure 41 – A graphical comparison of model and experimental emissions results

For experimental thermal efficiency and predicted temperature values, there was a roughly linear trend. As the predicted zone and maximum temperatures increased in the model, thermal efficiency values increased in the experiment. A caveat was that design 3b had slightly higher improvements in zone and maximum temperature than design 1a, with design 1a having a higher experimental thermal efficiency. These results suggest that the tool thermal predictions may be representative of actual flame conditions and can be a good way to make design decisions.

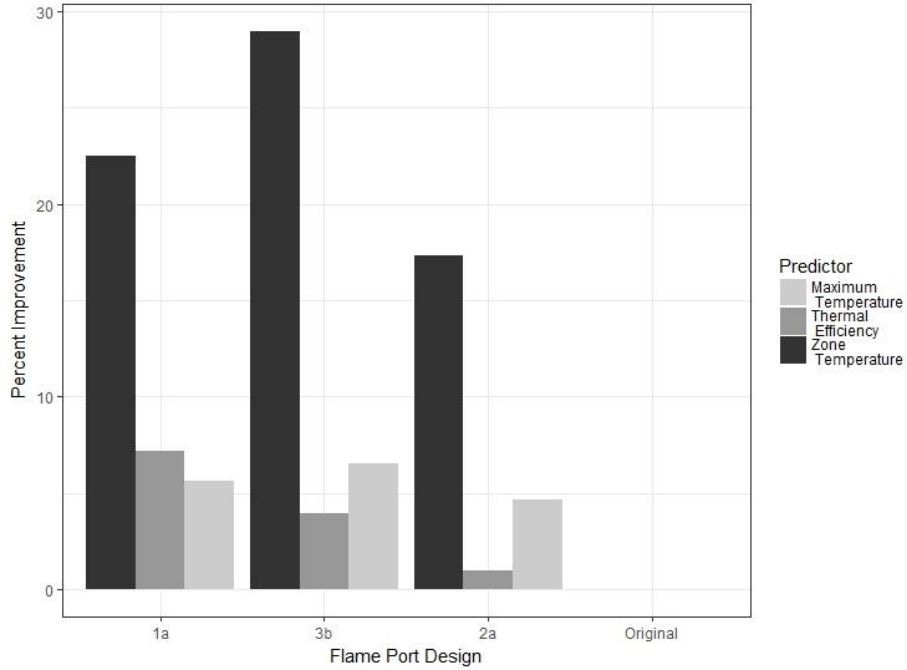


Figure 42 – A graphical comparison of model and experimental thermal results

Multivariate Regression Analysis

Similar to the method performed in Section 4.1.3, the Matlab® rstool was used to understand if a relationship could be measured between the design factors and experimental predictors. Since bulk flow rate was not measured, density and velocity of the gas mixture were unknown for the experiments. Therefore, only hydraulic diameter and port spacing were used as factors. The following hypothesis tests were conducted (n = 4).

$$H_0: \frac{\partial \text{thermal efficiency}}{\partial D_h, \partial \text{spacing}} = 0, H_0: \frac{\partial \text{combustion efficiency}}{\partial D_h, \partial \text{spacing}} = 0, H_0: \frac{\partial \text{total hydrocarbons}}{\partial D_h, \partial \text{spacing}} = 0, \\ \text{and } H_0: \frac{\partial \# \text{ of blue pixels}}{\partial D_h, \partial \text{spacing}} = 0$$

Out of the eight hypothesis tests conducted, none of the null hypotheses could be rejected. There were no significant relationships found between the factors and experimental predictors (p > 0.1), thus preventing the creation of a useful response surface tool. With a higher sample size, perhaps relationships could be established and a useful response surface created.

Tier Performance

Each of the four flame port geometry designs for the Lotus burner were compared against each other using the IWA tier structure. The repetitive low firepower, time controlled tests suggest that each design falls into the highest tier for both efficiency and emissions; Tier 4. The question becomes, was the increase in thermal efficiency for designs 1a and 3b an overall benefit even though emissions also increased? Since carbon monoxide emissions were in Tier 4 for all four designs, emissions are not of acute and immediate concern, but can still have long term consequences. Although severe exposure to carbon monoxide is well understood, the effects on health of prolonged, but low level exposure are unclear [54]. Long term, low level exposure can have subtle effects on the brain, contribute to heart disease and lead to low birth weight of newborns [54].

From a user standpoint, these health impacts are more difficult to quantify than the money and time savings associated with fuel reduction and a decreased time to boil. Increases in thermal efficiency have noticeable and immediate impacts on the user and in this study emissions for each design are marginal compared to most improved biomass cookstoves [52]. Thus, decisions on flame port geometry by an entrepreneur will likely be made in favor of thermal efficiency.

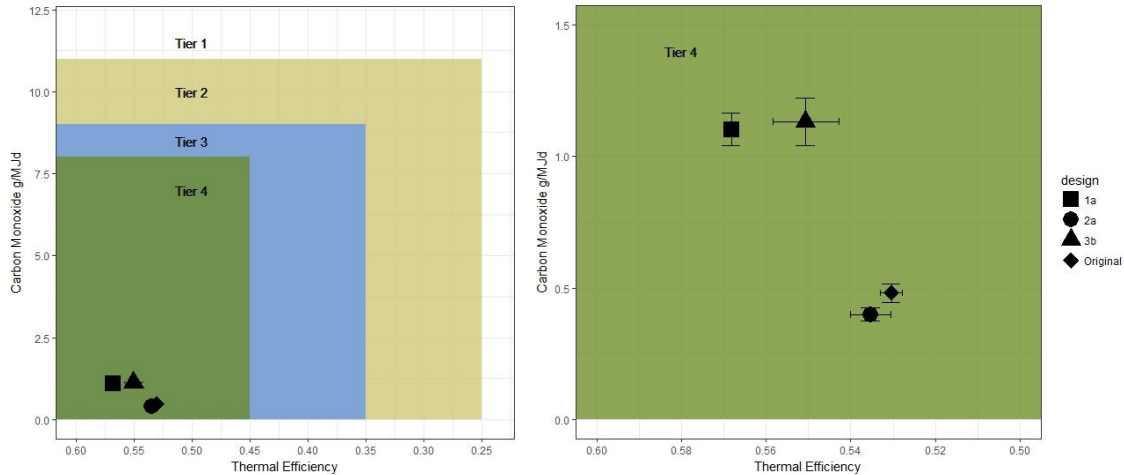


Figure 43 – Lower firepower time controlled design comparison using the IWA tier structure

4.2.2.2 Firepower Sweep

The firepower sweep tests were conducted to understand how thermal efficiency and emissions changed over a range of firepower from roughly 0.5 to 3.0 kW. The following results are displayed for trend analysis and were exploratory.

Thermal Efficiency

Experimental thermal efficiency data from each design was fitted quadratically to represent a parabolic trend with firepower ($n = 15$). Thermal efficiency reached a maximum at a specific point and decreased as firepower deviated from that point. The trend in the magnitude of maximum thermal efficiency roughly followed that of the above low firepower tests; design 1a ranking first, 3b second and 2a and the original tied for last. An interesting point from the sweep tests was that this hierarchy changes slightly with firepower. The results suggest that compared to the other designs, design 2a has a shallower decline in thermal efficiency away from the vertex and eventually converges with and at times outperforms designs 1a and 3b. Refer to the explanation of the flame photos (Section 4.2.2.1), in which the thought that Design 2a may be entraining more air than 1a and 3b was discussed. At firepower settings further away from the optimal, the increase in comparative combustion efficiency for design 2b may have outweighed the consequence of an

increased thermal mass. This may be especially true for firepower settings above the optimal, where as fuel flow rate increases, velocities at the ports increase, leading to a desire to have a phi value closer to one to limit flame lift-off.

The sweep data also suggests that thermal efficiency variance among designs is not consistent with firepower. In other words, changes to flame port geometry has varying degrees of impact on thermal efficiency at different firepower settings. For example, at the optimal firepower setting, the gap between the thermal efficiency of designs 1a and 2a is the largest. As firepower diverges from that setting, the gap distance changes and at one point becomes inverted in favor of design 2a. The takeaway here is that the degree of thermal efficiency superiority between designs is not constant with firepower.

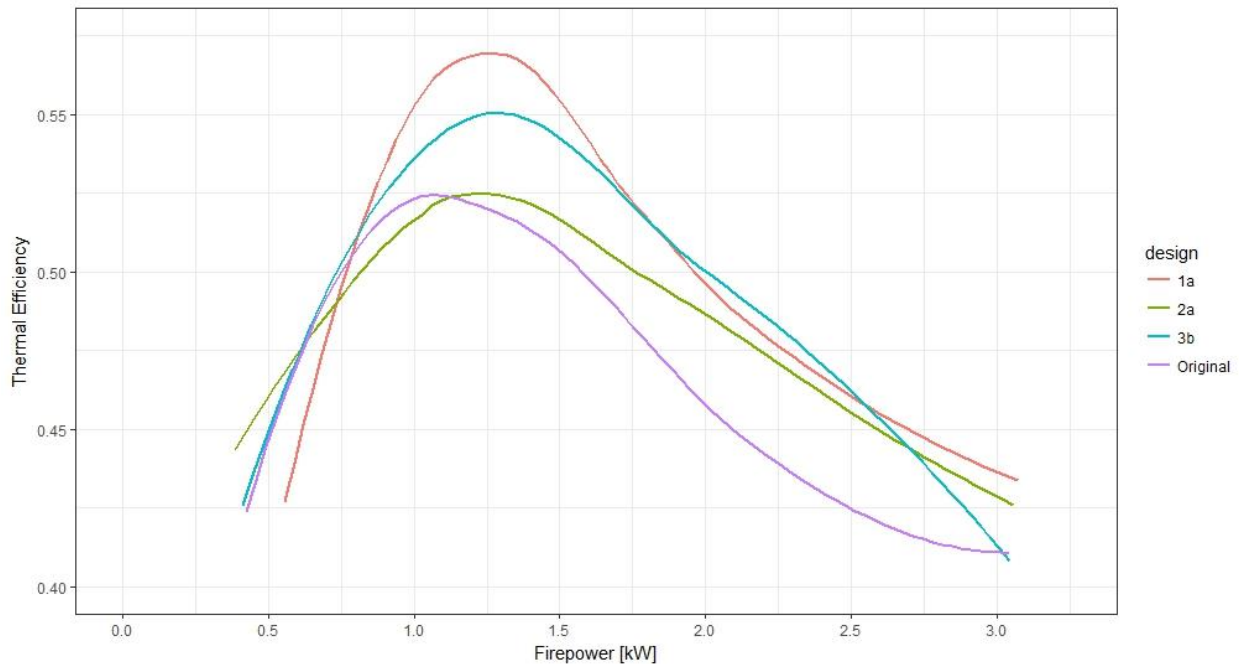


Figure 44 – Sweep thermal efficiency data overlain with best fit trendlines

Emissions

Carbon monoxide, total hydrocarbons and combustion efficiency data were fitted with linear trendlines. As firepower increased, emissions increased and the modified combustion

efficiency decreased. Designs 2a and the original had lower emissions and higher combustion efficiency for the majority of the sweep, which was likely due to a comparatively lower phi.

The overall emission trends found in the sweep were expected. With an increase in fuel flow rate and thus firepower, the velocity out of the flame ports increases. With a constant laminar flame speed, higher bulk flow velocities at the port push the stoichiometric mixture front further and further from the port surface, causing flame lift off. With a greater occurrence and degree of flame lift, an increasing amount of unburned hydrocarbons is allowed to escape into the emissions stream. Another consequence of higher bulk velocity is that a hydrocarbon is less likely to fully convert to carbon dioxide during combustion, leading to an increase in carbon monoxide.

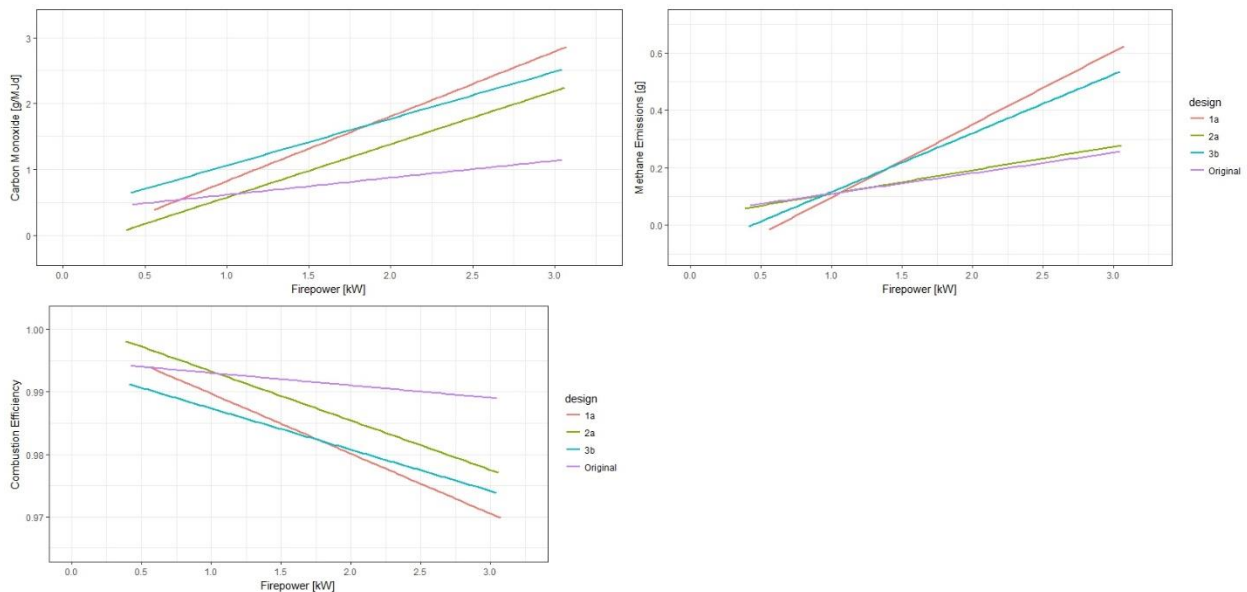


Figure 45 – Sweep emissions data overlain with linear trendlines

Tier Performance

The emissions for all the tests of each design fell within Tier 4. The majority of the tests for each design fell within Tier 4 for thermal efficiency. A few tests at the lower and higher end of the firepower spectrum fell into Tier 3.

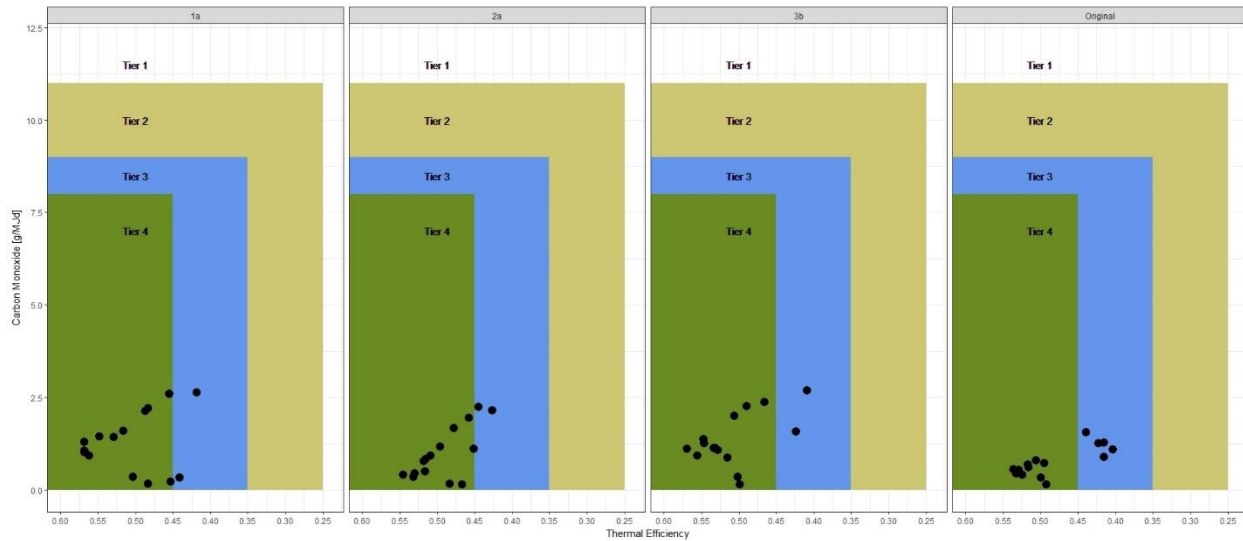


Figure 46 – Firepower sweep time controlled design comparison using the IWA tier structure

4.2.3 Temperature Controlled Protocol

To further justify the use of the time controlled protocol in place of the standard IWA methods, temperature controlled water boil tests were conducted for each of the four Lotus designs. The firepower of each temperature controlled test was matched to the test with the closest firepower setting from the time controlled firepower sweep. The percent error between the two protocols was calculated for three emissions categories (CO, CO₂ and total hydrocarbons) and thermal efficiency. From Figure 47, carbon dioxide and thermal efficiency translated well between protocols. Conversely, carbon monoxide and total hydrocarbons varied significantly. The contrast between the percent error of the predictors is likely a function of magnitude. Since carbon monoxide and total hydrocarbon concentrations were marginal in comparison to carbon dioxide, small fluctuations with respect to the total emissions stream became represented as large individual errors. Inherently, achieving a low percent error for a component that is a small percent of the total is difficult.

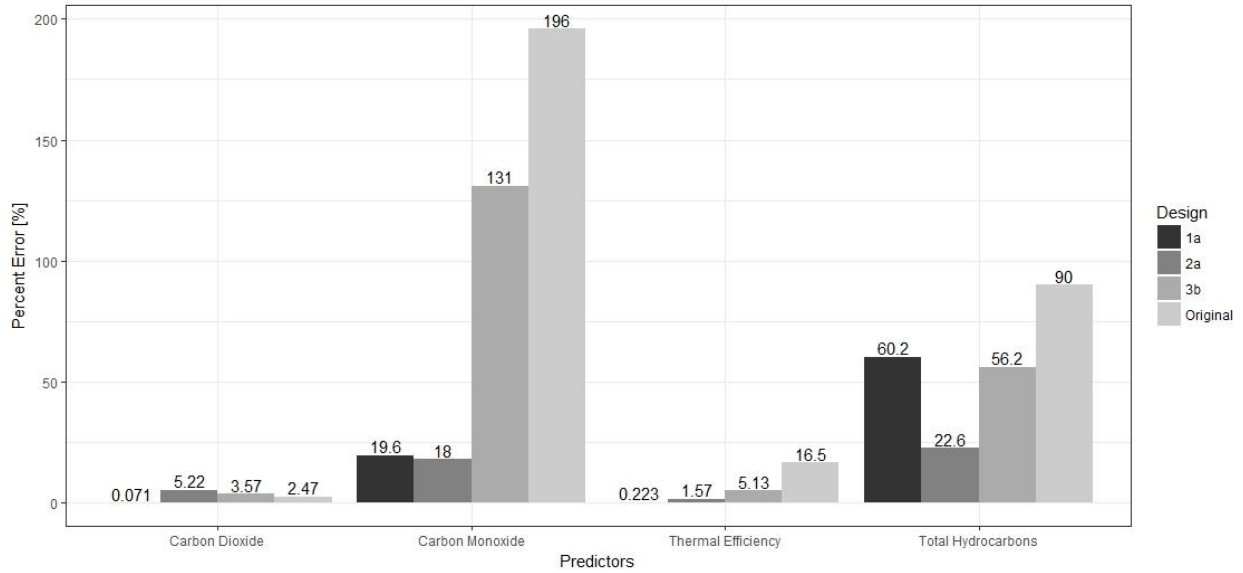


Figure 47 – A percent error comparison of the temperature and time controlled protocol

Sample size for the comparison was $n = 1$ for each protocol. Hence, the explanation above is suggestive and not conclusive. Expansion of the sample size for each protocol at matching firepower settings is required to confirm that a time controlled protocol can be a justifiable replacement for the standard IWA water boil test method.

CHAPTER 5. CONCLUSION

5.1 Summary of Findings

Flame port geometry was found to have a quantifiable influence upon the thermal efficiency and emissions of the Lotus biogas burner. Using the developed modeling tool, the significance of that influence was simulated and was corroborated using laboratory experiments. By applying multivariate regression modeling to the factors and predictors of the tool, linear relationships between port geometry and burner performance were developed to guide future burner design efforts. Specifically, hydraulic diameter (which inversely relates to the port dimension ratios), bulk velocity, and mixture density were used as factors that can be varied by a designer to achieve the desired predictor results. Overall, the results of the combined modeling tool and physical experiments suggest that the tool is an effective way to design for thermal efficiency, but has a low predictive power for emissions.

With regards to the original Lotus biogas burner, two port shape geometry designs were identified that noticeably improved thermal efficiency compared to the original. Design 1a, comprised of four mm circular ports, led the four (three newly developed and the original) Lotus flame port designs in thermal efficiency. Following closely behind was Design 3b, which was a mixture of rectangular slots and four mm circular ports. The success of four mm ports aligns with prior biogas studies, and the success of circular ports over the solely rectangular port design of 2a resonates with a NASA study showing an eight percent higher heat transfer coefficient in circular ports compared to rectangles [55]. Emissions for the Lotus burner, regardless of the port design and firepower setting, were securely positioned in the highest IWA tier, Tier 4. Since gaseous

burners tend to have higher combustion efficiencies, practitioner flame port design decisions may be made in favor of improving thermal efficiency.

Experimentation of off-the-shelf biogas burners suggested that flame type and firepower setting influences both thermal efficiency and emissions as stated by prior LPG and natural gas research. At an upper firepower setting, diffusion flames tended to achieve higher thermal efficiencies at the consequence of emitting higher concentrations of carbon monoxide and unburned hydrocarbons. At the same setting, entraining air to create a partially premixed flame tended to drastically improve the efficiency of combustion, while marginally decreasing thermal efficiency. In both flame type cases, turning down the power of the flame and hence decreasing Reynolds number, emissions decreased and thermal efficiency changed in a parabolic fashion, increasing then decreasing after a narrow plateau. These exploratory trends surrounding thermal efficiency support the conclusion made by Viskanta et al. that the type of flame and Reynolds number influence convective heat transfer [56].

This study provided evidence that suggests standard IWA temperature controlled water boil tests can be substituted with a 10-minute time controlled test for gaseous burners. Reduced testing time can reduce project costs and accelerate future research.

5.2 Original Hypotheses

At the onset of this study, the following hypotheses were created and tested. The extent of acceptance or rejection of both are discussed below each.

1. *Modern engineering software tools can accurately and effectively guide biogas burner flame port design.*

Software packages such as ANSYS®, Chemkin®, SolidWorks®, RStudio® and Matlab® were integral to the development of useful flame port designs. Each package played a specific role

and together they effectively guided the design process. Software tools were able to accurately predict thermal efficiency performance in the laboratory, but were ineffective in predicting emissions performance.

2. *By making analysis-guided alterations to the shape, spacing and configuration of burner flame ports, the thermal and combustion efficiency of biogas burners can be improved.*

Both the modeling tool and physical experiments suggested that the applied flame port geometry changes led to improvements in thermal efficiency for the Lotus burner. The modeling tool suggested an improvement in combustion efficiency that was not validated by the laboratory experiments. Combustion efficiency is a function of the emissions, and as previously discussed, is difficult to model. Unlike biomass cookstoves, combustion efficiency in gaseous burners often approaches 100%, so there is relatively little room for improvement.

5.3 Future Work

5.3.1 Modeling Tool Development

A significant weakness of the modeling tool was the limited spatial region for the combustion reaction, resulting in several emissions species failing to achieve mass continuity. Even though a larger reaction region leads to extended run times, achieving continuity may lead to an improved ability of the tool to predict emissions. Within the combustion reaction, the addition of heat transfer to a pot of water in the simulation would allow for the calculation of thermal efficiency, a predictor with direct comparison to laboratory testing. Recall that in this study, zone and maximum flame temperatures were used as a proxy to thermal efficiency.

Simulations completed thus far within the tool have been conducted at a single mass flow across each of the 10 designs (nine newly developed and the original). Further work that includes a range of simulated mass flow rates can strengthen relationships between the tool and laboratory

tests. As a result of greater simulation sample sizes, a more robust surface modeling tool could be built to guide future designers. A more confident and valuable design tool may then warrant the development of a graphical user interface for widespread adoption.

Moving beyond flame port geometry, the modeling tool can be leveraged to test the significance of modifying other portions of a burner. Design components to be tested include injector diameter and geometry, air entrainment placement, equivalence ratio, mixing tube length and diameter, total port area and configuration of the burner manifold. Including hydrogen sulfide in the combustion reaction could be another input to modify, which could potentially increase calorific value due to the presence of more hydrogen.

5.3.2 Experiments

The modeling tool cut out significant manufacturing and testing costs, but in the end experiments are required to validate simulation predictions. Increasing the sample size for the experiments conducted may lead to greater confidence in the results and may turn relationships into correlations and suggestions into conclusions. Further testing should aim to achieve population means to be within five percent of the sample mean 80 percent of the time [44].

To vary the mass flow rate from the high pressure gas cylinder, a manual pressure regulator was used, leading to difficulty in setting the flow to achieve a desired firepower. Significant quantities of gas and testing time were exhausted in the process. Even with a conscious effort to locate a specific firepower, the manual procedure introduced error that could be avoided with automation. Although mass flow controllers are costly, the flow automation they provide would minimize deviation and drastically reduce the time required to achieve a desired firepower setting.

A mass flow controller would enable the ability to perform a series of rapid succession firepower sweep tests across the collected burners. Performance data across a range of firepower settings for multiple burners will allow for deeper side by side comparisons. Between the Lotus and Rupak for example. Such comparisons will guide practitioner decision making when evaluating which burner is appropriate for a specific application.

If heat transfer to a pot of water is not added to the tool, zone and flame temperatures can be recorded experimentally to provide a directly compared predictor to the tool. An array of K-Type thermocouples can be constructed spanning the x, y and z axes to gather data for each test. A similar procedure was conducted by Basu et al. which enabled the development of a temperature contour map above an LPG burner [17].

5.3.3 Flame Port Design

Further design combinations of rectangular slots and circular ports are needed to solidify port geometry's influence upon the predictors. In this study, four mm circles and eight by four mm rectangular slots were the highest ranked for each shape in the tool, but with a greater selection, this may change. For instance, the other six designs simulated that were not chosen for manufacture, could have performed well in the laboratory. There is also a chance that these six designs perform worse than the original in the lab, even though they ranked higher in the simulation. This is indicated by the similar lab performance between design 2a and the original.

An alternative ranking method could also be applied to the simulated flame port design results. Rather than the simplified approach taken, the full Derringer and Suich method could be applied, potentially changing the rank of the ten designs and pulling a design different than the three chosen in this study into the top three. Adding sophistication into the ranking procedure was

beyond the scope of the present study but may better account for variations in predictor values between designs.

A critical design point to address is the expansion of the range in optimal thermal efficiency. The results of the time controlled firepower sweep showed a steep and nearly immediately decline in thermal efficiency when moving firepower to the left or right. A design that broadens a burner's ability to have high thermal efficiency at a greater range of firepower settings is needed. Beyond slots and circular ports, expanding channel designs are of interest to achieve this, as displayed in a port geometry patent issued to Maughan and General Electric [20]. At high firepower settings, these channel retention flames reduce bulk velocity through the length of an individual port and thus reduce the tendency for lift. Investigating the application of this design theory from LPG and natural gas to low pressure biogas would be worthwhile.

BIBLIOGRAPHY

- [1] International Energy Agency, Ed., *World energy outlook 2016*. Paris: OECD, 2016.
- [2] J. Otte and Food and Agriculture Organization of the United Nations, Eds., *Livestock sector development for poverty reduction: an economic and policy perspective: livestock's many virtues*. Rome: Food and Agricultural Organization of the United Nations, 2012.
- [3] M. C. Mapako, A. (Abel) Mbewe, and S. Habtetsion, *Renewables and energy for rural development in Sub-Saharan Africa*. Zed Books, 2004.
- [4] J. J. Lewis *et al.*, "Biogas Stoves Reduce Firewood Use, Household Air Pollution, and Hospital Visits in Odisha, India," *Environ. Sci. Technol.*, vol. 51, no. 1, pp. 560–569, Jan. 2017.
- [5] V. Tumwesige, L. Haroff, A. Apsley, S. Semple, and J. Smith, "Feasibility study assessing the impact of biogas digesters on indoor air pollution in households in Uganda.," presented at the Innovating Energy Access for Remote Areas, University of California Berkeley, 2015.
- [6] International Energy Agency, "Chapter 15 - Energy for Cooking in Developing Countries," in *World Energy Outlook 2006*, 2006.
- [7] J. Wang, "Decentralized Biogas Technology of Anaerobic Digestion and Farm Ecosystem: Opportunities and Challenges," *Front. Energy Res.*, vol. 2, 2014.
- [8] L. Sasse, "Biogas plants," *Vieweg Sohn Wiesb.*, 1988.
- [9] V. Tumwesige, D. Fulford, and G. C. Davidson, "Biogas appliances in Sub-Sahara Africa," *Biomass Bioenergy*, vol. 70, pp. 40–50, Nov. 2014.
- [10] A. J. Marchese, "Chemical Equilibrium Course Pack," in *Combustion*, Colorado State University, 2015.
- [11] I. Glassman, R. A. Yetter, and N. G. Glumac, *Combustion*. Academic Press, 2014.
- [12] L. Gattei, "A study on the fluid dynamics of domestic Gas burners," alma, 2009.
- [13] D. J. Zube, "Heat transfer efficiency of biomass cookstoves," Colorado State University Libraries, 2010.
- [14] H. R. N. Jones, *The Application of Combustion Principles to Domestic Gas Burner Design*. Taylor & Francis, 1989.
- [15] J. C. Griffiths and E. J. Weber, *The design and application of impingement target burners*. American Gas Association Laboratories, 1957.
- [16] J. A. Harris and R. South, *Gas Engineering and Management*. Institution of Gas Engineers., 1978.
- [17] D. Basu, R. Saha, R. Ganguly, and A. Datta, "Performance Improvement of LPG Cookstoves through burner and nozzle modifications," *J. Energy Inst.*, vol. 81, no. 4, pp. 218–225, 2008.
- [18] S. Tia *et al.*, "Effect of Burner Type on Thermal Efficiency and Emission of LPG Cookstoves," *Month*, vol. 18, no. 1, 2007.
- [19] H. B. Li, T. T. Wong, C. W. Leung, and S. D. Probert, "Thermal performances and CO emissions of gas-fired cooker-top burners," *Appl. Energy*, vol. 83, no. 12, pp. 1326–1338, Dec. 2006.
- [20] J. R. Maughan, "Atmospheric gas burner assembly for improved flame retention and stability," US5899681 A, 04-May-1999.
- [21] D. Fulford, "Biogas Stove Design: A Short Course," Kingdom Bioenergy Ltd, Aug. 1996.

- [22] M. P. Jadhav and D. S. S. Sudhakar, "Analysis of Burner for Biogas by Computational Fluid Dynamics and Optimization of Design by Genetic Algorithm," 2015.
- [23] D. Fulford, "History of Biogas Burners," Jul-2016.
- [24] A. Chandra, G. N. Tiwari, V. K. Srivastava, and Y. P. Yadav, "Performance evaluation of biogas burners," *Energy Convers. Manag.*, vol. 32, no. 4, pp. 353–358, 1991.
- [25] A. Chandra, G. N. Tiwari, and Y. P. Yadav, "Hydrodynamical modelling of a biogas burner," *Energy Convers. Manag.*, vol. 32, no. 4, pp. 395–401, 1991.
- [26] SNV Netherlands Development Organisation, K. C. Khandelwal, and V. Gupta, "Popular Summary of the Test Reports on Biogas Stoves and Lamps prepared by testing institutes in China, India and the Netherlands." Feb-2009.
- [27] I. N. Itodo, G. E. Agyo, and P. Yusuf, "Performance evaluation of a biogas stove for cooking in Nigeria," *J. Energy South. Afr.*, vol. 18, no. 3, p. 15, 2007.
- [28] David Olubiyi Obada, Anthony Iheanyichukwu Obi, Muhammed Dauba, and Fatai Olukayode Anafi, "Design and Construction of a Biogas Burner," *Palest. Tech. Univ. Res. J.*, pp. 35–42, Sep. 2014.
- [29] A. K. Kurchania, N. L. Panwar, and S. D. Pagar, "Development of domestic biogas stove," *Biomass Convers. Biorefinery*, vol. 1, no. 2, pp. 99–103, May 2011.
- [30] Y.-C. Ko and T.-H. Lin, "Emissions and efficiency of a domestic gas stove burning natural gases with various compositions," *Energy Convers. Manag.*, vol. 44, no. 19, pp. 3001–3014, Nov. 2003.
- [31] C. Ghenai and I. Janajreh, "Combustion of Renewable Biogas Fuels," *Editor. Board Memb.*, p. 831, 2015.
- [32] J. Prapas, M. E. Baumgardner, A. J. Marchese, B. Willson, and M. DeFoort, "Influence of chimneys on combustion characteristics of buoyantly driven biomass stoves," *Energy Sustain. Dev.*, vol. 23, pp. 286–293, Dec. 2014.
- [33] Gregory P. Smith, David M. Golden, Michael Frenklach, Nigel W. Moriarty, Boris Eiteneer, Mikhail Goldenberg, C. Thomas Bowman, Ronald K. Hanson, Soonho Song, William C. Gardiner, Jr., Vitali V. Lissianski, and Zhiwei Qin, *GRI-Mech 3.0*. University of California Berkeley: Gas Research Institute.
- [34] D. E. Ward and W. Hao, "Projections of emissions from burning of biomass for use in studies of global climate and atmospheric chemistry," 1991.
- [35] G. Derringer and R. Suich, "Simultaneous Optimization of Several Response Variables," *J. Qual. Technol.*, vol. 12, pp. 214–219, 1980.
- [36] J. Prapas, "Toward the understanding and optimization of chimneys for buoyantly driven biomass stoves," Colorado State University. Libraries, 2007.
- [37] S. F. Baldwin, *Biomass stoves: engineering design, development, and dissemination*. Arlington, Va., USA : Princeton, N.J., USA: Volunteers in Technical Assistance ; Center for Energy and Environmental Studies, Princeton University, 1987.
- [38] K. J. Chae, A. Jang, S. K. Yim, and I. S. Kim, "The effects of digestion temperature and temperature shock on the biogas yields from the mesophilic anaerobic digestion of swine manure," *Bioresour. Technol.*, vol. 99, no. 1, pp. 1–6, Jan. 2008.
- [39] A. P. Grieshop, J. D. Marshall, and M. Kandlikar, "Health and climate benefits of cookstove replacement options," *Energy Policy*, vol. 39, no. 12, pp. 7530–7542, Dec. 2011.
- [40] i3D Mfg., *Lotus Burner Flame Port Designs*. 2016.
- [41] IWA, "The Water Boiling Test," Global Alliance for Clean Cookstoves, 2014.

- [42] Kelsey Bilsback, Kelley Hixson, and Michael Johnson, “A Novel Approach to Cookstove Testing: The Firepower Sweep Test,” 30-Jan-2015.
- [43] Y. Wang, M. D. Sohn, Y. Wang, K. M. Lask, T. W. Kirchstetter, and A. J. Gadgil, “How many replicate tests are needed to test cookstove performance and emissions? — Three is not always adequate,” *Energy Sustain. Dev.*, vol. 20, pp. 21–29, Jun. 2014.
- [44] C. L’Orange, D. Leith, J. Volckens, and M. DeFoort, “A quantitative model of cookstove variability and field performance: Implications for sample size,” *Biomass Bioenergy*, vol. 72, pp. 233–241, Jan. 2015.
- [45] T. Turányi, L. Zalotai, S. Dóbé, and T. Bérces, “Effect of the uncertainty of kinetic and thermodynamic data on methane flame simulation results,” *Phys. Chem. Chem. Phys.*, vol. 4, no. 12, pp. 2568–2578, 2002.
- [46] S. Kong and R. D. Reitz, “Numerical study of premixed HCCI engine combustion and its sensitivity to computational mesh and model uncertainties,” *Combust. Theory Model.*, vol. 7, no. 2, pp. 417–433, Jun. 2003.
- [47] T. T. Wong, C. W. Leung, D. Y. Liu, and H. B. Li, “Application of multi-objective neural-network optimization to gas-fired cooktop design,” 2007.
- [48] B. Moffitt, T. Bradley, D. Mavris, and D. Parekh, “Design Space Exploration of Small-Scale PEM Fuel Cell Long Endurance Aircraft,” in *6th AIAA Aviation Technology, Integration and Operations Conference (ATIO)*, American Institute of Aeronautics and Astronautics.
- [49] T. T. Wong, C. W. Leung, and M. C. Wong, “Sustainable Design of Impinging Premixed Slot Jets,” *World Acad. Sci. Eng. Technol. Int. J. Mech. Aerosp. Ind. Mechatron. Manuf. Eng.*, vol. 4, no. 8, pp. 696–700, 2010.
- [50] R. Grewal, J. A. Cote, and H. Baumgartner, “Multicollinearity and Measurement Error in Structural Equation Models: Implications for Theory Testing,” *Mark. Sci.*, vol. 23, no. 4, pp. 519–529, Nov. 2004.
- [51] M.C. Wong, T.T. Wong, and C.W. Leung, “Modeling of Impinging Premixed Multi-slot Jet Efficiency and Greenhouse Gas Emissions,” presented at the 7th Asia-Pacific Conference on Combustion, Taipei, Taiwan, 2009, p. 245.
- [52] J. Tryner, “Combustion phenomena in biomass gasifier cookstoves,” Colorado State University. Libraries, 2016.
- [53] K. R. Smith, R. Uma, V. V. N. Kishore, J. Zhang, V. Joshi, and M. A. K. Khalil, “Greenhouse Implications of Household Stoves: An Analysis for India,” *Annu. Rev. Energy Environ.*, vol. 25, no. 1, pp. 741–763, 2000.
- [54] C. L. Townsend and R. L. Maynard, “Effects on health of prolonged exposure to low concentrations of carbon monoxide,” *Occup. Environ. Med.*, vol. 59, no. 10, pp. 708–711, Oct. 2002.
- [55] J. N. Livingood and P. Hrycak, “Impingement heat transfer from turbulent air jets to flat plates: a literature survey,” 1973.
- [56] R. Viskanta, “Heat transfer to impinging isothermal gas and flame jets,” *Exp. Therm. Fluid Sci.*, vol. 6, no. 2, pp. 111–134, Feb. 1993.

APPENDIX A. SUPPLEMENTARY MATERIAL FOR CHAPTERS 1, 2 AND 3

Chemkin Lookup Table

Table 15 – Lookup table produced by Chemkin for a 60 mole percent biogas

Biogas Mixture	Equivalence Ratio (Phi)	Laminar Flame Speed (SL)	Adiabatic Flame Temperature (K)
CH4-0.6 / CO2-0.4	0.6	8.5	1594
CH4-0.6 / CO2-0.4	0.7	14.2	1750
CH4-0.6 / CO2-0.4	0.8	19.5	1893
CH4-0.6 / CO2-0.4	0.9	23.4	2017
CH4-0.6 / CO2-0.4	1	25.3	2100
CH4-0.6 / CO2-0.4	1.1	24.3	2061
CH4-0.6 / CO2-0.4	1.2	20.0	1973
CH4-0.6 / CO2-0.4	1.3	12.5	1885
CH4-0.6 / CO2-0.4	1.4	6.4	1802
CH4-0.6 / CO2-0.4	1.5	4.6	1732

Carbon Mass Balance Method

(1) Sources of carbon in biogas: methane (CH₄) and carbon dioxide (CO₂)

$$\frac{0.6 \text{ moles of } CH_4}{1 \text{ mole of biogas}} * MW_{CH_4}(16) = \frac{9.6 \text{ grams of } CH_4}{1 \text{ mole of biogas}}$$

$$\frac{0.4 \text{ moles of } CO_2}{1 \text{ mole of biogas}} * MW_{CO_2}(44) = \frac{17.6 \text{ grams of } CO_2}{1 \text{ mole of biogas}}$$

$$\frac{9.6 \text{ grams of } CH_4}{1 \text{ mole of biogas}} + \frac{17.6 \text{ grams of } CO_2}{1 \text{ mole of biogas}} = MW_{biogas} (27.2)$$

$$\frac{9.6 \text{ grams of } CH_4}{1 \text{ mole of biogas}} * \frac{1}{MW_{biogas}(27.2)} = \text{mass fraction of } CH_4 \text{ in biogas (0.353)}$$

$$\frac{17.6 \text{ moles of } CO_2}{1 \text{ mole of biogas}} * \frac{1}{MW_{biogas}(27.2)} = \text{mass fraction of } CO_2 \text{ in biogas (0.647)}$$

$$\begin{aligned} & \text{mass fraction of } CH_4 \text{ in biogas (0.353)} * \frac{12 \text{ grams of carbon in } CH_4}{\text{molecular mass of } CH_4(16)} \\ & + \text{mass fraction of } CO_2 \text{ in biogas(0.647)} * \frac{12 \text{ grams of carbon in } CO_2}{\text{molecular mass of } CO_2(44)} \\ & = \text{mass fraction of Carbon in biogas (44.1 \% for 60 mol\% methane 40 mol\% carbon dioxide)} \end{aligned}$$

(2) Sources of carbon in the emissions stream

$$\text{Carbon in Methane (CH}_4\text{): } NDIR \text{ grams of methane} * \frac{\text{grams of carbon in } CH_4}{\text{molecular mass of } CH_4} = \text{grams of carbon}$$

$$\text{Carbon in Carbon Dioxide (CO}_2\text{): } NDIR \text{ grams of carbon dioxide} * \frac{\text{grams of carbon in } CO_2}{\text{molecular mass of } CO_2} = \text{grams of carbon}$$

$$\text{Carbon in Carbon Monoxide (CO): } NDIR \text{ grams of carbon monoxide} * \frac{\text{grams of carbon in } CO}{\text{molecular mass of } CO} = \text{grams of carbon}$$

Total carbon in emissions stream = sum of the three above carbon values

(3) Amount of fuel consumed

$$\frac{\text{Total carbon in emissions stream}}{\text{mass fraction of carbon in biogas (43.6 \% for 60 mol\% methane 40 mol\% carbon dioxide)}}$$

Mixing Simulation Background Calculations

Using the equivalence ratio calculated in the mixing simulation, other parameters were calculated to verify the port exit velocity prediction generated by ANSYS Fluent®. The process occurred as follows.

- (1) Percent of the Stoichiometric Air was calculated from equivalence ratio

$$\% \text{ of Stoich Air} = \frac{100}{\Phi}$$

- (2) Fraction of air needed to meet stoichiometric mixing before combustion

$$a_{stoich} = \left[\frac{1 \text{ mole of C in biogas}}{1 \text{ mole of C in methane}} + \frac{2.4 \text{ moles of H in biogas}}{4 \text{ moles of H in methane}} \right] - \left[\frac{0.8 \text{ moles of O in biogas}}{2 \text{ moles of O in O}_2} \right]$$

- (3) Fraction of actual air entrained

$$a = \% \text{ of Stoich Air} * \frac{a_{stoich}}{100}$$

- (4) Number of moles of air entrained per mole of fuel provided

$$\frac{\text{Moles of Air}}{\text{Mole of Fuel}} = 4.76 * a$$

- (5) The mole fractions of the air and fuel

$$\text{mole fraction of air} = \frac{\text{moles of air entrained}}{\text{moles of air entrained} + 1 \text{ mole of fuel provided}}$$

$$\text{mole fraction of fuel} = \frac{1 \text{ mole of fuel provided}}{\text{moles of air entrained} + 1 \text{ mole of fuel provided}}$$

- (6) Now that the bulk flow composition is understood, the volumetric flow rates of fuel and air can be calculated via the continuity equation

$$\dot{V}_{fuel}[LPM] = A_{XS, fuel inlet}[cm^2] * v_{inlet} \left[\frac{cm}{s} \right] * \frac{60s}{1 \text{ min}} * \frac{1 L}{1000 cm^3}$$

$$\dot{V}_{air}[LPM] = \text{mole fraction of air} * \frac{\dot{V}_{fuel}[LPM]}{\text{moles fraction of fuel}}$$

- (7) Using biogas and air density, mass flow rate can be calculated

$$\dot{m}_{fuel} \left[\frac{kg}{s} \right] = \dot{V}_{fuel}[LPM] * \frac{60 s}{1 \text{ min}} * \rho_{biogas} \left[\frac{kg}{m^3} \right] * \frac{1 m^3}{1000 L}$$

$$\dot{m}_{air} \left[\frac{kg}{s} \right] = \dot{V}_{air} [LPM] * \frac{60 s}{1 min} * \rho_{air} \left[\frac{kg}{m^3} \right] * \frac{1m^3}{1000 L}$$

(8) By leveraging the bulk mass flow rate and total port cross sectional area, exit velocity of the fuel and air mixture can be calculated.

$$\dot{m}_{bulk} \left[\frac{kg}{s} \right] = \dot{m}_{fuel} \left[\frac{kg}{s} \right] + \dot{m}_{air} \left[\frac{kg}{s} \right]$$

$$v_{port\ exit} \left[\frac{cm}{s} \right] = \frac{\dot{m}_{bulk} \left[\frac{kg}{s} \right]}{\rho_{mixture} \left[\frac{kg}{m^3} \right] * A_{xs,singular\ port} [cm^2] * \# of\ ports * \frac{1m^3}{100^3 cm^3}}$$

Flame Color Analysis

```
## Thomas J Decker
## February 28, 2017
## Flame photo analysis

library(png)
library(grid)
library(gridExtra)
library(plyr)
library(pixmap)
library(Matrix)

##read in the no pot photo
original <- readPNG("original_png_nopot.png")
onea <- readPNG("onea_png_nopot.png")
twoa <- readPNG("twoa_png_nopot.png")
threeb <- readPNG("threeb_png_nopot.png")

#####
#Flame images when no pot is suppressing the flame
#####

##reshape no pot images into a data frame
df_original = data.frame(red = matrix(original[,1], ncol=1),
                        green = matrix(original[,2], ncol=1),
                        blue = matrix(original[,3], ncol=1))

df_onea = data.frame(red = matrix(onea[,1], ncol=1),
                    green = matrix(onea[,2], ncol=1),
                    blue = matrix(onea[,3], ncol=1))

df_twoa = data.frame(red = matrix(twoa[,1], ncol=1),
                    green = matrix(twoa[,2], ncol=1),
                    blue = matrix(twoa[,3], ncol=1))





df_threeb = data.frame(red = matrix(threeb[,1], ncol=1),
                      green = matrix(threeb[,2], ncol=1),
                      blue = matrix(threeb[,3], ncol=1))

#Calculate count of non-zero values in blue column of no pot images

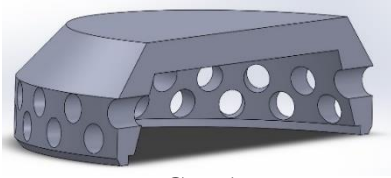
nonzero <- function(x) sum(x != 0)
numcolwise(nonzero)(df_original)
```

```
numcolwise(nonzero)(df_onea)  
numcolwise(nonzero)(df_twoa)  
numcolwise(nonzero)(df_threeb)
```

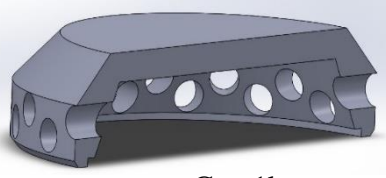
Off the Shelf Burners

Burner	Photo
<p>Lotus Phnom Penh, Cambodia Distributed by the National Biogas Programme Manufactured by The Development Technology workshop</p>	
<p>Dual Swirl Burner Shenzhen, China Distributed and Manufactured by Puxin Tech</p>	
<p>Single Burner New Delhi, India Distributed and Manufactured by Rupak Enterprises</p>	
<p>Dual Burner Goliath Mexico City, Mexico Distributed and Manufactured by Delher</p>	

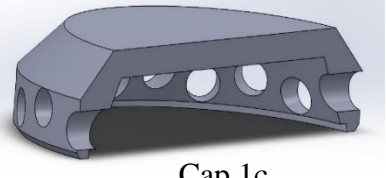
Cap Design Snapshots



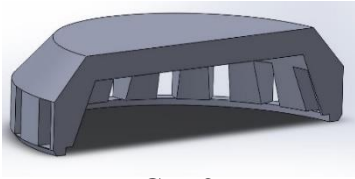
Cap 1a



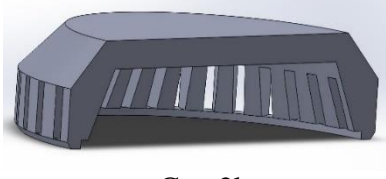
Cap 1b



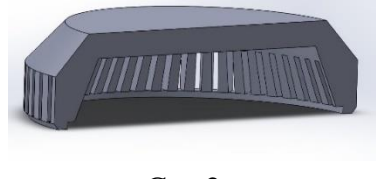
Cap 1c



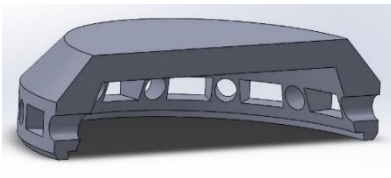
Cap 2a



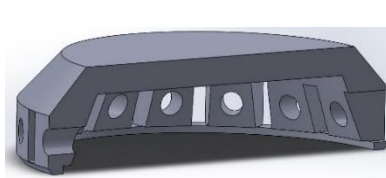
Cap 2b



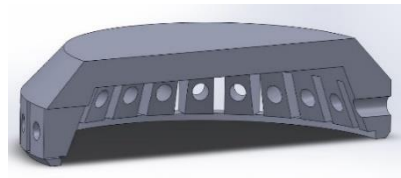
Cap 2c



Cap 3a



Cap 3b



Cap 3c

APPENDIX B. SUPPLEMENTARY MATERIAL FOR CHAPTER 4

Particulate Matter Data

Table 16 – Summary of particulate matter results

Stove	Firepower [kW]	Flame Type	Filter Measurement [μg]	LOD	Met ?	LOQ	Met ?	Total PM [g/kg]
Lotus	1	premix	24.67	12.69	Yes	34.14	No	NA
Lotus	1	premix	52.3		Yes		Yes	0.102
Lotus	1	diffusion	20.67		Yes		No	NA
Lotus	1	diffusion	20.67		Yes		No	NA
Lotus	4.5	premix	31.33		Yes		No	NA
Lotus	4.5	premix	51.33		Yes		Yes	0.045
Lotus	4.5	diffusion	32		Yes		No	NA
Lotus	4.5	diffusion	13.33		Yes		No	NA
Lotus	4.5	diffusion	5.67		No		No	NA

Delher LPG Stove Modifications

Off the shelf LPG burners are equipped with injectors specific to the properties of LPG. In the case of the Delher Goliath LPG burner, low pressure (less than 0.5 psi) biogas could not overcome the pressure drop across the two injectors (inner and outer), making the off the shelf configuration incompatible with decentralized biogas. To reduce the pressure drop, the injector diameters were expanded. Guided by a design ratio of injector cross sectional area to total port area, three scenarios were created. Each scenario resulted in successful combustion of low pressure biogas.

Table 17 – Delher LPG stove modifications for biogas

Delher 1 – High Area Ratio	Delher 2 – Mid Area Ratio	Delher 3 – Low Area Ratio
Original flame ports, both injectors drilled out to 1/4"	Original flame ports, inner injector drilled out to 1/16", outer injector drilled out to 5/64"	Original inner flame ports, outer flame ports drilled out to 7/64", inner injector drilled out to 1/16", outer injector drilled out to 7/64"

Each scenario was tested using the temperature controlled protocol at an upper firepower setting. The scenarios were evaluated using both diffusion and premixed flames. By reducing the area ratio, thermal efficiency was improved and emissions reduced with premixed flames. The first scenario with a diffusion flame fell into Tier 1 for thermal efficiency, with the remaining falling into Tier 2. All tests fell into Tier 4 for emissions. Explained in Section 4.2.1.1, the Rupak and Puxin biogas burners achieved Tier 3 for efficiency at the same upper firepower setting, outperforming each of the Delher scenarios.

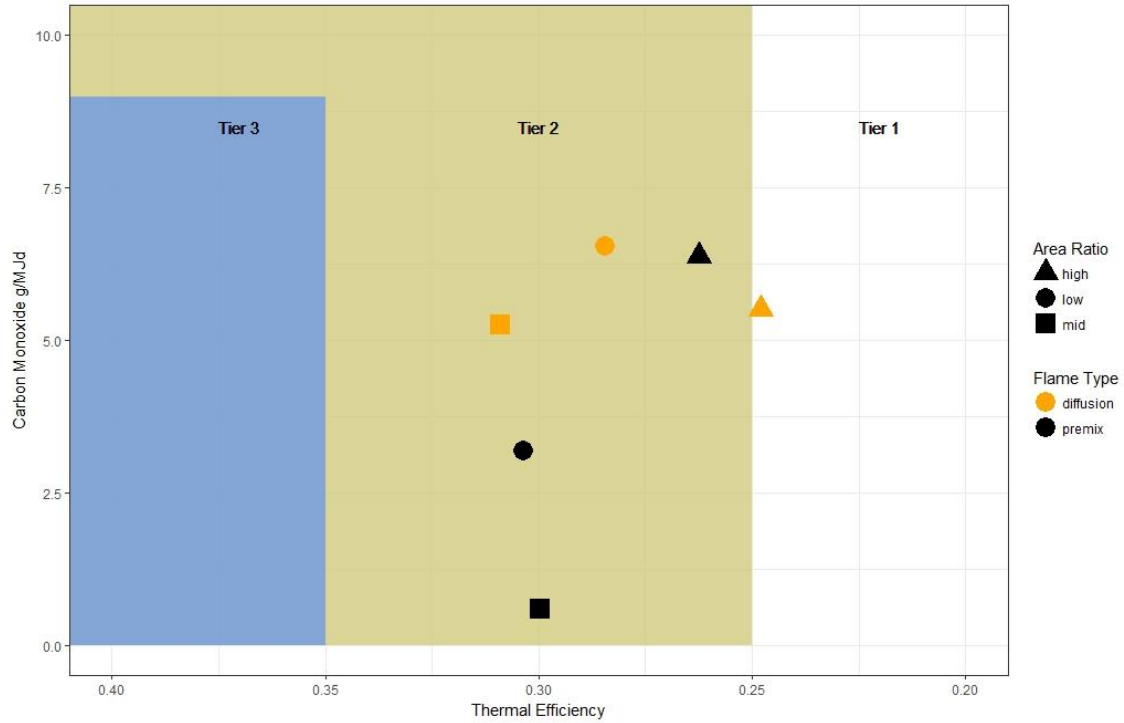


Figure 48 – Delher LPG modification IWA tier comparison

Using the same ranking procedure described in Section 3.2.6, the three scenarios were stacked against each other. The third scenario with a premixed flame ranked the highest. Further testing at a low firepower setting may reaffirm which Delher scenario is preferred for low pressure biogas.

Table 18 – Delher scenario ranking comparison

RANKING TABLE							
Design	Fire power (kW)	Flame Type	Time to Boil (min)	Thermal Efficiency (%)	Combustion Efficiency (%)	Total Hydrocarbon (g)	Total
Delher 1	4.40	Diffusion	5	6	3	3	17
Delher 1	4.45	Premix	6	5	5	6	22
Delher 2	4.20	Diffusion	2	1	4	2	9
Delher 2	4.20	Premix	4	3	1	5	13
Delher 3	4.35	Diffusion	3	4	6	4	17
Delher 3	4.44	Premix	1	2	2	1	6